

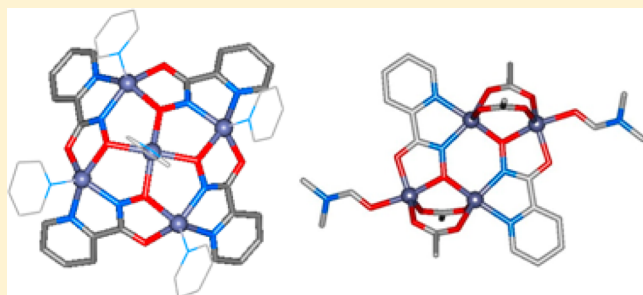
Isolation of Elusive Tetranuclear and Pentanuclear M(II)–Hydroxamate Intermediates in the Assembly of Lanthanide [15-Metallacrown-5] Complexes

Joseph Jankolovits, Jeff W. Kampf, and Vincent L. Pecoraro*

Department of Chemistry, University of Michigan, Ann Arbor, 930 North University Avenue, Ann Arbor, Michigan 48109-1055, United States

Supporting Information

ABSTRACT: Two intermediates in the assembly of lanthanide metallacrowns (MCs) of divalent transition metals and ligands in the picoline hydroxamic acid (picHA)/ α -amino hydroxamic acid family were synthesized and crystallographically characterized. Structures of the elusive $M^{II}[12-MC_{M^II,L-4}]^{2+}$ were obtained with $M = Ni, Zn$ and $L = picHA, quinaldic\ hydroxamic\ acid$. Consistent with previous calculations, the complex is highly concave, particularly with $Zn(II)$. ESI-MS and 1H NMR reveal that the complexes retain their structure in solution. The $Zn(II)$ analogue reacts with $Ln(III)$ ions to form $Ln^{III}[15-MC_{Zn(II),picHA-5}]^{3+}$ in pyridine. The greater stability of $Zn^{II}[12-MC_{Zn(II),picHA-4}]^{2+}$ relative to the $Cu(II)$ and $Ni(II)$ analogues is inferred and attributed to the square-pyramidal $Zn(II)$ ions being complementary with the concave MC topology. A $Zn_4(picHA)_2(OAc)_4(DMF)_2$ species bearing a tetranuclear $[6-MC_{Zn^II,picHA-2}]$ motif was also isolated. A mechanism for $M^{II}[12-MC_{M^II,L-4}]^{2+}$ formation is proposed on the basis of structural analysis of tetranuclear $[6-MC_{M^II,L-2}]$ complexes. These results contribute to the goal of controlling the reactivity of intermediates in the assembly of lanthanide MCs, and coordination driven macrocycles in general, to prepare complexes with greater stability or enhanced physical properties.



INTRODUCTION

Research on coordination-driven assemblies has given rise to vast libraries of compounds with novel structural topologies, physical properties, and molecular recognition behavior.¹ Molecular recognition by coordination-driven assemblies has been utilized in sensing, separations, and catalysis.² The promise of coordination-driven assemblies in these varied applications has motivated broad synthetic efforts to prepare novel assemblies with functional topologies. Furthermore, a better understanding of assembly dynamics is sought to aid in the expansion of synthetic methodologies for these complexes. In particular, novel methodologies could be useful for isolating motifs that might be thermodynamically or kinetically unstable.^{3,4}

Metallacrowns (MCs) are a benchmark class of coordination-driven assembly with a macrocyclic motif that structurally and functionally resemble crown ethers (Figure 1).^{5–8} MCs were historically some of the first coordination-driven assemblies,^{9–12} and many of these complexes exhibit benchmark single-molecule magnetism^{13–15} or luminescence,¹⁶ recognize guest molecules,^{17–19} or serve as building blocks for porous solids.^{20–22} From a self-assembly standpoint, $M^N[15-MC_{M^N,L-5}]^{23}$ complexes derived from α -aminohydroxamic acids (α -aminoHA) or picoline hydroxamic acid (picHA) ligands (Figure 2) are a particularly well developed three-component system.^{24,25} These $M^N[15-MC_{M^N,L-5}]$ complexes have been

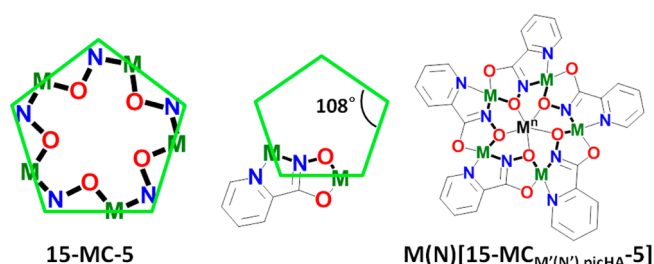


Figure 1. Diagram displaying the design strategy for $M^N[15-MC_{M^N,L-5}]$ complexes based on the chelate ring geometry. The pentagonal $M^N[15-MC_{M^N,L-5}]$ is generated from ligands that form fused five-membered chelate rings, such as picHA.

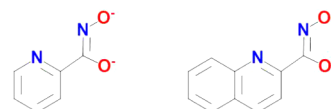


Figure 2. Chemdraw representations of picHA (left) and quinHA (right).

Received: December 23, 2012

prepared with Ni(II), Cu(II), and Zn(II) ring ions.^{26–29} $M^N[15-MC_{M^{N,L}}-5]$ assembles in the presence of a large cation that is complementary with the ~ 1.05 Å radius central cavity, such as Ln(III) ions, UO_2 , Pb(II), and Ca(II) central ions. The stability and versatility of the pentagonal $M^N[15-MC_{M^{N,L}}-5]$ originates from the geometric optimization of the fused five-membered chelate rings in picHA and α -aminoHA ligands. The chelate rings are oriented at 108° internal angles, making them the appropriate vertex for a planar pentagonal molecule (Figure 1).²⁴ Beyond the fundamentals of molecular assembly, interest in $M^N[15-MC_{M^{N,L}}-5]$ has also focused on their magnetic properties,³⁰ selective guest binding,^{31–33} and formation of dimeric compartments.^{34,35} These compartments have led to crystalline host–guest complexes exhibiting second-harmonic generation³⁶ and chiral mesochannels.³⁷

For $M^N[15-MC_{M^{N,L}}-5]$ complexes, the speciation of the ligand and ring ions in the absence of an appropriate central ion has been intensely studied.³⁸ This topic addresses fundamental aspects of three-component assemblies and also the role of guest molecules in self-assembly. Additionally, the issue has an interesting historical context in relation to crown ethers. In the absence of a cationic guest, the oxygen atoms on flexible crown ethers are known to orient toward the periphery of the macrocycle to avoid unfavorable electrostatic interactions between the oxygen lone pairs.³⁹ For $M^N[15-MC_{M^{N,L}}-5]$ complexes, the fused chelate rings prevent this reorganization of the oxygen atoms. Unfavorable interactions between the oxygen lone pairs are thought to prevent the formation of a vacant $M^N[15-MC_{M^{N,L}}-5]$ using Cu(II) and Zn(II) ring ions and ligands in the picHA/ α -aminoHA family, though data for such a complex have been obtained with Ni(II).⁴⁰ On the basis of extensive mass spectrometry, potentiometry, and calorimetry data, $M^{II}[12-MC_{M^{II,L}}-4]$ has been identified as the primary intermediate in the assembly of $M^N[15-MC_{M^{N,L}}-5]$ complexes with Cu(II) and Ni(II).^{40–44} DFT calculations predict that the $Cu^{II}[12-MC_{Cu^{II},\alpha\text{-aminoHA}}-4]^{2+}$ complex possesses a strained, concave structure.⁴⁵ Despite extensive effort, no $M^{II}[12-MC_{M^{II,L}}-4]^{2+}$ has been characterized crystallographically with ligands from the picHA/ α -aminoHA family. Instead, complexes resembling collapsed metallacrowns with tetranuclear $[6-MC_{M^{II,L}}-2]$ motifs, such as $Cu^{II}_4(\text{picHA})_4$ ⁴⁶ and a $Cu^{II}_{28}(\text{norvalineHA})_{20}$ metallahelicate,⁴⁷ have been obtained from organic solvents. These complexes are thought to result from a complicated solvent-dependent solution and crystallization equilibrium, where $M^{II}[12-MC_{M^{II,L}}-4]^{2+}$ is a major solution species. In other planar systems, collapsed metallacrowns have been reported.^{14,48,49}

In this work, the first crystal structures of the elusive $M^{II}[12-MC_{M^{II,L}}-4]^{2+}$ ($M = \text{Zn(II), Ni(II)}$) with a ligand from the picHA/ α -aminoHA family are reported, and their solution stability and role as intermediates in the formation of $\text{Ln}^{III}[15-MC_{M^{III},\text{picHA}}-5]^{3+}$ complexes are described. Additionally, a tetranuclear $[6-MC_{Zn^{II},\text{picHA}}-2]$ complex, $Zn^{II}_4(\text{picHA})_2(\text{acetate})_4(\text{DMF})_2$, is presented that forms the basis for a proposed mechanism for the assembly of $M^{II}[12-MC_{M^{II,L}}-4]^{2+}$. The implications of these compounds in understanding and controlling the assembly of lanthanide metallacrowns and other three-component coordination-driven assemblies are discussed.

EXPERIMENTAL SECTION

All reagents were obtained from commercially available sources and used as received unless discussed otherwise. Picoline hydroxamic acid

was synthesized according to the previously reported procedure.¹⁶ Where specified, methanol was dried by distillation over magnesium. Electrospray ionization mass spectrometry (ESI-MS) was performed on a Micromass LCT time-of-flight electrospray ionization mass spectrometer at 150°C at a cone voltage of 50 V. Samples were injected via syringe pump as ~ 50 μM solutions. ESI-MS data were processed with MassLynx 4.0 software. NMR was performed on 400 or 500 MHz Varian spectrometers, and the chemical shifts were referenced to residual solvent signals. ^1H Diffusion NMR was performed using a DOSY gradient compensated stimulated echo with spin lock and convection compensation (DgcsstSL_cc) pulse sequence at temperatures of 293 K in pyridine- d_5 . A diffusion delay of 150 ms, a diffusion gradient length of 3.0 ms, and a gradient strength array of 15–30 increments were used. The gradient field strength was calibrated with D_2O by the University of Michigan NMR facility staff. The data was fit according to the equation $\ln(I/I_0) = -\gamma^2\delta^2G^2(\Delta - \delta/3)D$ to solve for the diffusion coefficient (D), where I = intensity or integral of the peak at a given G , I_0 = intensity or integral of the peak at $G = 0$, γ = magnetogyric constant of the nucleus (for ^1H , $g = 2.675 \times 108 \text{ T}^{-1} \text{ s}^{-1}$), δ = diffusion gradient length, Δ = diffusion delay, and G = gradient field strength.

Quinaldic Hydroxamic Acid. In a dry 250 mL flask, quinaldic acid (6g, 0.0319 mol) was mixed with 100 mL of dry methanol under N_2 in an ice bath. Thionyl chloride (0.0478 mol, 3.46 mL) was added dropwise, making the solution homogeneous. The solution was refluxed for 20 h, cooled to room temperature, and evaporated to dryness under vacuum, yielding quinaldic acid methyl ester hydrochloride as an off-white powder. This solid was dissolved in 30 mL of degassed methanol, combined with a solution of potassium hydroxide (0.0319 mol, 2.06 g) in 30 mL of degassed methanol under a stream of N_2 , and cooled in an ice bath for 15 min. Separately, solutions of hydroxylamine hydrochloride (0.0957 mol, 6.65 g) and potassium hydroxide (0.0957 mol, 6.19 g) in degassed methanol were prepared under a stream of N_2 , combined, and cooled in an ice bath for 15 min. The ester and hydroxylamine solutions were filtered to remove the white potassium chloride precipitate. The filtrates were combined, flushed with N_2 , stoppered, and stirred for 2 days at room temperature. An additional 3 equiv of hydroxylamine was prepared from hydroxylamine hydrochloride and potassium hydroxide as described above and added to the reaction mixture. After 2 more days, the reaction mixture was concentrated to a volume of ~ 50 mL and the solid was triturated to break up and dissolve the yellow solid, though a colorless solid (potassium chloride) remained. A 425 mL portion of water was slowly added, leading to the precipitation of quinaldic hydroxamic acid as white needles and dissolution of the potassium chloride. The solution was cooled in an ice bath, and the solid was collected by vacuum filtration and rinsed with cold water. The white solid was ground to a fine powder and thoroughly dried in a vacuum desiccator over P_2O_5 . Yield: 4.90 g, 82%. Mp: 144°C dec. ^1H NMR (δ (ppm); 400 MHz, CD_3OD): 8.46 (d, 1H, $J = 8$ Hz), 8.14 (m, 2H), 7.98 (d, 1H, $J = 8$ Hz), 7.82 (td, 1H), 7.68 (td, 1H). ^{13}C NMR (δ (ppm); 100 MHz): 163.0, 149.3, 146.6, 137.4, 130.0, 129.3, 129.2, 127.6, 127.6, 118.1. IR (cm^{-1}): 3416 (O–H, br), 3135 (N–H, br), 2861 (C–H), 1664 (s), 1648 (s), 1625 (s), 1504 (s), 1424 (w), 1043 (m), 918 (m), 769 (w), 626 (w). Anal. Found (calcd for $\text{C}_{10}\text{H}_8\text{N}_2\text{O}_2$): C, 63.95 (63.83); H, 4.18 (4.29); N, 14.87 (14.89).

$Zn^{II}[12-MC_{Zn^{II},\text{picHA}}-4](\text{OTf})_{1.25}(\text{OH})_{0.75}$. PicHA (1.086 mmol, 150.0 mg) and zinc triflate (1.358 mmol, 493.5 mg) were mixed with 10 mL of methanol and 1 mL of pyridine in a 125 mL Erlenmeyer flask. Triethylamine (2.172 mmol, 302.9 μL) was added, and the solution was stirred for 1 h. Ether (75 mL) was added all at once, resulting in a yellow-white precipitate. The flask was covered, and faintly yellow crystals formed after sitting overnight. The crystals were isolated by filtration and rinsed with 3 mL of -20°C methanol, giving about 210 mg of solid. This material was recrystallized by dissolving in 3 mL of 4/1 methanol/pyridine, precipitating with 30 mL of ether, and letting the slurry sit overnight in a stoppered flask. The solid was collected by filtration, rinsed with 2 mL of -20°C methanol, and air-dried. Yield: 116.7 mg, 26%. ^1H NMR (δ (ppm); 500 MHz, $\text{C}_5\text{D}_5\text{N}$): 8.87 (d, 1H, $J = 5$ Hz), 8.39 (d, $J = 8$ Hz, 1H), 8.04 (t, 1H, $J = 8$ Hz).

Table 1. Crystallographic Data and Refinement Details for $\text{Zn}^{\text{II}}[12\text{-MC}_{\text{Zn}^{\text{II}},\text{picHA-4}}](\text{OTf})_{1.25}(\text{OH})_{0.75}$, $\text{Zn}^{\text{II}}[12\text{-MC}_{\text{Zn}^{\text{II}},\text{quinHA-4}}](\text{BF}_4)_2$, $\text{Ni}^{\text{II}}[12\text{-MC}_{\text{Ni}^{\text{II}},\text{quinHA-4}}](\text{NO}_3)_2$, and $\text{Zn}_4(\text{picHA})_2(\text{OAc})_4$

	$\text{Zn}^{\text{II}}[12\text{-MC}_{\text{Zn}^{\text{II}},\text{picHA-4}}](\text{OTf})_{1.25}(\text{OH})_{0.75}$	$\text{Zn}^{\text{II}}[12\text{-MC}_{\text{Zn}^{\text{II}},\text{quinHA-4}}](\text{BF}_4)_2$	$\text{Ni}^{\text{II}}[12\text{-MC}_{\text{Ni}^{\text{II}},\text{quinHA-4}}](\text{NO}_3)_2$	$\text{Zn}_4(\text{picHA})_2(\text{OAc})_4(\text{DMF})_2$
mol formula	$\text{Zn}_{10}\text{C}_{107.75}\text{H}_{112}\text{F}_{7.5}\text{N}_{27}\text{O}_{34.75}$	$\text{Zn}_5\text{C}_{87.5}\text{H}_{75.90}\text{B}_2\text{F}_8\text{N}_{17.5}\text{O}_{10.2}$	$\text{Ni}_5\text{C}_{98.75}\text{H}_{85.25}\text{N}_{10.88}\text{O}_{19.25}$	$\text{Zn}_4\text{C}_{26}\text{H}_{34}\text{N}_6\text{O}_{14}$
mol wt	3217.59	2036.23	2025.83	916.15
cryst syst/space group	triclinic/ <i>P</i> 1	monoclinic/ <i>P</i> 2 ₁ / <i>c</i>	triclinic/ <i>P</i> $\bar{1}$	triclinic/ <i>P</i> $\bar{1}$
<i>a</i> (Å)	13.9392 (3)	20.048 (4)	13.1078 (2)	7.9774 (2)
<i>b</i> (Å)	14.4645 (3)	23.873 (3)	15.7214 (2)	10.4943 (3)
<i>c</i> (Å)	19.5726 (14)	18.784 (3)	21.3430 (15)	1036971 (3)
α (deg)	83.760 (6)	90	85.346 (6)	80.681 (1)
β (deg)	89.320 (6)	93.190 (18)	85.445 (6)	77.535 (1)
γ (deg)	74.143 (5)	90	85.262 (6)	79.547 (1)
<i>V</i> (Å ³)	3773.0 (3)	8976 (3)	4357.0 (3)	852.85 (4)
<i>Z</i> /density, ρ (g cm ⁻³)	1/1.416	4/1.507	2/1.544	1/1.784
μ (mm ⁻¹), <i>F</i> (000)	2.758/1633	1.402/4148	1.858/2096	2.853/464
cryst size (mm ³)	0.20 × 0.16 × 0.12	0.16 × 0.08 × 0.08	0.18 × 0.06 × 0.01	0.34 × 0.20 × 0.20
θ range for data collection (deg)	3.2–68.24	1.75–26.39	2.08–68.23	1.97–30.52
limiting indices	–16 ≤ <i>h</i> ≤ 16 –17 ≤ <i>k</i> ≤ 17 –23 ≤ <i>l</i> ≤ 23	–25 ≤ <i>h</i> ≤ 25 –29 ≤ <i>k</i> ≤ 29 –23 ≤ <i>l</i> ≤ 23	–15 ≤ <i>h</i> ≤ 15 –18 ≤ <i>k</i> ≤ 18 –23 ≤ <i>l</i> ≤ 25	–11 ≤ <i>h</i> ≤ 11 –14 ≤ <i>k</i> ≤ 14 –15 ≤ <i>l</i> ≤ 15
no. of meas/unique reffns	80841/24956	104052/18365	127732/15677	34139/5208
completeness to θ (%)	97.7	99.9	98.3	99.9
no. of data/restraints/params	24956/2719/2147	18365/485/1315	15677/186/1288	5208/0/230
goodness of fit on <i>F</i> ²	1.046	1.041	1.182	1.044
final <i>R</i> indices (<i>I</i> > 2 σ (<i>I</i>))	<i>R</i> 1 = 0.0699, <i>wR</i> 2 = 0.2113	<i>R</i> 1 = 0.0552, <i>wR</i> 2 = 0.1512	<i>R</i> 1 = 0.0715, <i>wR</i> 2 = 0.2066	<i>R</i> 1 = 0.0225, <i>wR</i> 2 = 0.0594
<i>R</i> indices (all data)	<i>R</i> 1 = 0.0718, <i>wR</i> 2 = 0.2144	<i>R</i> 1 = 0.0888, <i>wR</i> 2 = 0.1762	<i>R</i> 1 = 0.0878, <i>wR</i> 2 = 0.2181	<i>R</i> 1 = 0.0260, <i>wR</i> 2 = 0.0612
largest diff peak and hole (e Å ⁻³)	1.435 and –0.998	1.059 and –0.621	1.940 and –0.828	0.684 and –0.289

ESI-MS (methanol): *m/z* 434.8²⁺ (434.9²⁺ calcd for $[\text{Zn}_5(\text{picHA})_4]^{2+}$), 1018.5⁺ (1017.7⁺ calcd for $[\text{Zn}_5(\text{picHA})_4(\text{OTf})]^{+}$). Anal. Found (calcd for $\text{Zn}_5(\text{C}_6\text{H}_4\text{N}_2\text{O}_2)_4(\text{OTf})_{1.25}(\text{OH})_{0.75}(\text{C}_5\text{H}_5\text{N})_6(\text{H}_2\text{O})_{2.5}$): C, 37.72 (37.93); H, 2.78 (2.96); N, 11.18 (10.96).

$\text{Zn}^{\text{II}}[12\text{-MC}_{\text{Zn}^{\text{II}},\text{quinHA-4}}](\text{BF}_4)_2$. quinHA (0.399 mmol, 75.0 mg) and zinc tetrafluoroborate hydrate (0.498 mmol, 128.0 mg) were mixed in 10 mL of a 4/1 methanol/pyridine mixture (v/v). Triethylamine (0.797 mmol, 111.2 μL) was added, and the solution was stirred overnight. The solution was transferred to a 50 mL beaker and placed in a wide-mouth jar containing ether (~75 mL). Long yellow needles crystallized upon ether vapor diffusion and were isolated by filtration, rinsed with –20 °C methanol, and air-dried. Yield: 86.1 mg, 51%. ESI-MS (methanol): *m/z* 534.9²⁺ (535.9²⁺ calcd for $[\text{Zn}_5(\text{quinHA})_4]^{2+}$). Anal. Found (calcd for $\text{Zn}_5(\text{C}_{10}\text{H}_6\text{N}_2\text{O}_2)_4(\text{BF}_4)_2(\text{C}_5\text{H}_5\text{N})_6$): C, 48.42 (48.25); H, 3.28 (3.09); N, 11.27 (11.25).

$\text{Zn}^{\text{II}}[12\text{-MC}_{\text{Zn}^{\text{II}},\text{quinHA-4}}](\text{NO}_3)_2$. quinHA (0.399 mmol, 75.0 mg) and zinc nitrate hexahydrate (0.498 mmol, 148.2 mg) were mixed in 10 mL of a 4/1 methanol/pyridine mixture (v/v). Triethylamine (0.797 mmol, 111.2 μL) was added, and the solution was stirred overnight. The solution was transferred to a 50 mL beaker, and the beaker was placed in a wide-mouth jar containing ether (~75 mL). Yellow-orange crystals formed by ether vapor diffusion. The crystals were isolated by filtration, rinsed with –20 °C methanol, and air-dried. Yield: 131.2 mg, 85%. ¹H NMR (δ (ppm); 400 MHz, CD₃OD): 8.77 (d, 1H, *J* = 9 Hz), 8.67 (d, *J* = 6 Hz, 1H), 8.32 (d, *J* = 8, 3H), 8.06 (d, 1H, *J* = 8 Hz), 8.01 (t, 1H, *J* = 8 Hz), 7.33 (t, 1H, *J* = 7 Hz). ESI-MS (methanol): *m/z* 535.1²⁺ (535.9²⁺ calcd for $[\text{Zn}_5(\text{quinHA})_4]^{2+}$), 1132.2⁺ (1132.8⁺ calcd for $[\text{Zn}_5(\text{quinHA})_4(\text{NO}_3)]^{+}$). Anal. Found (calcd for $\text{Zn}_5(\text{C}_{10}\text{H}_6\text{N}_2\text{O}_2)_4(\text{NO}_3)_2(\text{C}_5\text{H}_5\text{N})_4(\text{H}_2\text{O})_{2.5}$): C, 46.18 (46.28); H, 3.09 (3.17); N, 12.59 (12.59).

$\text{Ni}^{\text{II}}[12\text{-MC}_{\text{Ni}^{\text{II}},\text{quinHA-4}}](\text{NO}_3)_2$. quinHA (0.53 mmol, 100 mg) and nickel dinitrate hexahydrate (0.66 mmol, 193.2 mg) were mixed in 18 mL of pyridine. Triethylamine (1.06 mmol, 148.2 μL) was added, and the solution was heated to 65 °C for 24 h, resulting in the precipitation of a yellow powder. The mixture was cooled in a –20 °C freezer, and the powder was isolated by vacuum filtration, rinsed with 3 mL of cold

water, and air-dried. Yield: 137.4 mg, 60%. ESI-MS (DMSO): *m/z* 518.0²⁺ (518.0²⁺ calcd for $[\text{Ni}_5(\text{quinHA})_4]^{2+}$). Anal. Found (calcd for $\text{Ni}_5(\text{C}_{10}\text{H}_6\text{N}_2\text{O}_2)_4(\text{NO}_3)_2(\text{C}_5\text{H}_5\text{N})_5(\text{H}_2\text{O})_9$): C, 45.27 (45.40); H, 3.50 (3.93); N, 12.07 (12.22). Crystals of the complex suitable for crystal structure determination were grown from a solution of quinHA (0.11 mmol, 20 mg), nickel dinitrate hexahydrate (0.11 mmol, 47.4 mg), and *n*-butylamine (0.21 mmol, 21 μL) in 5 mL of pyridine. Once homogeneous, the sample was immediately set to crystallize by ether vapor diffusion. $\text{Ni}^{\text{II}}[12\text{-MC}_{\text{Ni}^{\text{II}},\text{quinHA-4}}](\text{NO}_3)_2$ crystallized as red-brown needles within 1 week.

$\text{Zn}_4(\text{picHA})_2(\text{acetate})_4(\text{DMF})_2$. Picoline hydroxamic acid (0.724 mmol, 100 mg), zinc acetate dihydrate (0.724 mmol, 158.9 mg), and europium nitrate pentahydrate (0.145 mmol, 62.1 mg) were stirred in 15 mL of methanol overnight. A 3 mL portion of DMF was added, and the solution was set to crystallize by slow evaporation. In 2 weeks, the faintly yellow crystals that formed were isolated by vacuum filtration, rinsed with –20 °C methanol, and air-dried. Yield: 37.2 mg, 22% based on Zn(II). ¹H NMR (δ (ppm); 500 MHz, C₅D₅N): 8.26 (d, 1H, *J* = 8 Hz), 8.09 (s, 1H), 7.74 (t, *J* = 8, 1H), 2.72 (s, 3.5H), 2.61 (s, 3.5H), 2.26 (s, 6.5 H). Anal. Found (calcd for $\text{Zn}_4(\text{C}_6\text{H}_4\text{N}_2\text{O}_2)_2(\text{C}_2\text{H}_3\text{O}_2)_2(\text{C}_3\text{H}_7\text{NO})_2$): C, 34.19 (34.09); H, 3.75 (3.74); N, 9.28 (9.17).

Crystallography. Intensity data for $\text{Zn}^{\text{II}}[12\text{-MC}_{\text{Zn}^{\text{II}},\text{picHA-4}}](\text{OTf})_{1.25}(\text{OH})_{0.75}$ and $\text{Ni}^{\text{II}}[12\text{-MC}_{\text{Ni}^{\text{II}},\text{quinHA-4}}](\text{NO}_3)_2$ were collected at 85(2) K on an AFC10K Saturn 944+ CCD-based X-ray diffractometer equipped with a low-temperature device and Micromax-007HF Cu-target microfocus rotating anode ($\lambda = 1.54187$ Å), operated at 0.20 kW power (20 kV, 10 mA) and $\mu = 4.510$ mm⁻¹. The data were processed with CrystalClear 2.0⁵⁰ and corrected for absorption. The structures were solved and refined with the SHELXTL (version 2008/4) software package.⁵¹

Intensity data for $\text{Zn}^{\text{II}}[12\text{-MC}_{\text{Zn}^{\text{II}},\text{quinHA-4}}](\text{BF}_4)_2$ and $\text{Zn}_4(\text{picHA})_2(\text{acetate})_4$ were collected at 85(2) K on a standard Bruker SMART-APEX CCD-based X-ray diffractometer equipped with a low-temperature device and fine-focus Mo-target X-ray tube ($\lambda = 0.71073$ Å) operated at 1500 W power (50 kV, 30 mA). The frames

were integrated with the Bruker SAINT⁵² software package with a narrow frame algorithm. The data were processed with SADABS⁵³ and corrected for absorption.

All structures were solved and refined with the Bruker SHELXTL software package.⁵⁴ All non-hydrogen atoms were refined anisotropically. Hydrogen atoms were placed in their idealized positions. All other experimental details are presented in Table 1.

RESULTS

Assembly and Structure of $\text{Zn}^{\text{II}}[12\text{-MC}_{\text{Zn}^{\text{II}},\text{L}}\text{-4}]^{2+}$. As a starting point, the reaction between Zn(II) and picHA was examined with ESI-MS. Similar to the Cu(II) and Ni(II) chemistry, ESI-MS of a 1/1 mixture of Zn(II) and picHA in pyridine revealed a $\text{Zn}_5\text{L}_4^{2+}$ species at 434.9²⁺, along with $\text{Zn}_5\text{L}_4(\text{anion})^+$ complexes (Figure 3). No other MC species of

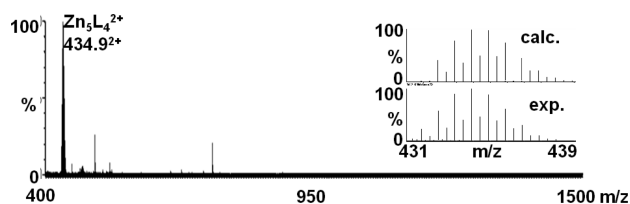


Figure 3. Mass spectra of the assembly of 1/2/1 H_2picHA (L), triethylamine, and $\text{Zn}(\text{NO}_3)_2$ in pyridine at room temperature after 24 h.

significant intensity were observed in pyridine. Zn_5L_4 was crystallized from a methanol/pyridine/ether suspension. X-ray crystallography revealed two independent $\text{Zn}^{\text{II}}[12\text{-MC}_{\text{Zn}^{\text{II}},\text{picHA}}\text{-4}](\text{py})_5^{2+}$ complexes in the unit cell with 2.5 triflate (OTf) and 1.5 hydroxide counterions (Figure 4). The picHA ligands form

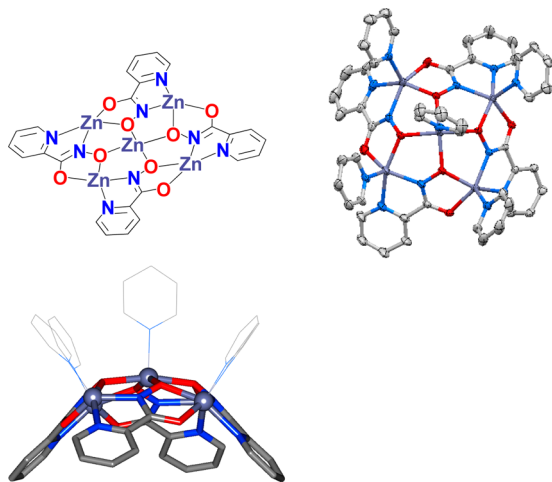


Figure 4. Chemdraw diagram (top left) and crystal structure images of the $\text{Zn}^{\text{II}}[12\text{-MC}_{\text{Zn}^{\text{II}},\text{picHA}}\text{-4}](\text{OTf})_{1.25}(\text{OH})_{0.75}$ complex viewed down the convex face (thermal ellipsoid plot, top right) and from the side (ball and stick diagram, bottom). Color scheme: gray, carbon; red, oxygen; blue, nitrogen; gray-purple, zinc. Coordinated pyridine ligands are displayed as thin lines in the ball and stick diagram for clarity.

fused five-membered chelate rings, coordinating in a bidentate fashion through the carbonyl and hydroximate oxygens at one position and bidentate through the hydroximate and pyridyl nitrogens at the other. This coordination motif is repeated four times, generating the $[12\text{-MC}_{\text{Zn}^{\text{II}},\text{picHA}}\text{-4}]$ motif with the familiar $[\text{M}-\text{N}-\text{O}]$ repeating unit. The Zn(II) ions are five-coordinate with an axially bound pyridine. The $\text{Zn}-\text{N}_{\text{picHA-pyridyl}}$ bond

distances average 2.152 Å, which is longer than expected. The other bond distances are typical for Zn(II) complexes (Table 2). τ values⁵⁵ were measured to assess whether the Zn(II) ions are square pyramidal or trigonal bipyramidal, where 0 represents pure square-pyramidal and 1 indicates pure trigonal-bipyramidal geometries (Table 2). The τ values range from 0.03 to 0.41, revealing that the Zn(II) ions have distorted-square-pyramidal geometries. The Zn(II) ions in the ring rest far above the equatorial ligand plane by an average of 0.581 Å. The central Zn(II) rests 0.325 Å above the oxygen mean plane (OMP). The central cavity has a radius averaging 0.67 Å, well suited for the late, first-row, divalent transition metals.

The complex as a whole possesses a concave topology, making it a metallocavitand.^{56,57} This bowl shape was predicted by Tegoni et al. for $\text{Cu}^{\text{II}}[12\text{-MC}_{\text{Cu}^{\text{II}},\alpha\text{-aminoHA}}\text{-4}]^{2+}$ complexes and observed in the $[12\text{-MC-4}]$ units in the recently reported $\text{Tb}^{\text{III}}[12\text{-MC}_{\text{Zn}^{\text{II}},\text{picHA}}\text{-4}]_2[24\text{-MC}_{\text{Zn}^{\text{II}},\text{picHA}}\text{-8}](\text{OTf})_3$ complex. The concave cavity is about 14 Å in diameter and 4.5 Å deep on the basis of the distance from the most distant picHA hydrogen atom to the OMP. The $\text{Zn}^{\text{II}}[12\text{-MC}_{\text{Zn}^{\text{II}},\text{picHA}}\text{-4}]^{2+}$ complex packs in the solid state in a herringbone pattern (Figure S1, Supporting Information). The convex faces interact primarily through extensive π -stacking interactions between the coordinated pyridines. The concave faces associate in a different layer, with the picHA ligands on one $\text{Zn}^{\text{II}}[12\text{-MC}_{\text{Zn}^{\text{II}},\text{picHA}}\text{-4}]^{2+}$ interacting with the edge of the cavity of another through π -stacking interactions. A methanol molecule is located within the center of the cavity at van der Waals distances from the $\text{Zn}^{\text{II}}[12\text{-MC}_{\text{Zn}^{\text{II}},\text{picHA}}\text{-4}]^{2+}$.

To demonstrate the versatility of the $\text{Zn}^{\text{II}}[12\text{-MC}_{\text{Zn}^{\text{II}},\text{L}}\text{-4}]^{2+}$ motif, a crystal structure was also obtained with quinaldic hydroxamic acid (quinHA, Figure 2), a derivative of picHA. The $\text{Zn}^{\text{II}}[12\text{-MC}_{\text{Zn}^{\text{II}},\text{quinHA}}\text{-4}](\text{pyridine})_5(\text{BF}_4)_2$ structure (Figure 5) shows effectively the same structural motif as the $\text{Zn}^{\text{II}}[12\text{-MC}_{\text{Zn}^{\text{II}},\text{picHA}}\text{-4}]^{2+}$ complex. The Zn(II) ions again have square-pyramidal geometries ($\tau = 0.04\text{--}0.30$) with axially bound pyridine ligands. Bond lengths fall within the expected values (Table 1), though again the $\text{Zn}^{\text{II}}-\text{N}_{\text{quinHA-pyridyl}}$ bond length is slightly elongated (2.16 Å). The central cavity radius of $\text{Zn}^{\text{II}}[12\text{-MC}_{\text{Zn}^{\text{II}},\text{quinHA}}\text{-4}](\text{BF}_4)_2$ is 0.646 Å, again providing a reasonable fit for the Zn(II) ion (ionic radius 0.68 Å). Due to the larger size of the quinHA ligand, the concave cavity has a greater maximum depth and width (4.8 and 18.7 Å, respectively). The cavity contains two pyridine molecules in the center (Figure S2, Supporting Information). Two unbound tetrafluoroborate anions in the lattice provide charge balance.

Synthesis and Structure of $\text{Ni}^{\text{II}}[12\text{-MC}_{\text{Ni}^{\text{II}},\text{quinHA}}\text{-4}](\text{NO}_3)_2$. A $\text{Ni}^{\text{II}}[12\text{-MC}_{\text{Ni}^{\text{II}},\text{quinHA}}\text{-4}](\text{NO}_3)_2$ complex was isolated as an amorphous powder by heating H_2quinHA , triethylamine, and $\text{Ni}(\text{NO}_3)_2$ in pyridine at 65 °C. Crystals suitable for structural characterization were obtained from a pyridine solution by ether vapor diffusion. The ligand coordination is almost identical with that of $\text{Zn}^{\text{II}}[12\text{-MC}_{\text{Zn}^{\text{II}},\text{quinHA}}\text{-4}](\text{NO}_3)_2$ (Figure 6). The Ni(II) ring ions are octahedral with axial pyridine ligands, while the central Ni(II) is square-pyramidal ($\tau = 0.08$). The complex as a whole is slightly bowled, with the depth of the concave face being a modest 1.29 Å. The central cavity radius is a mere 0.57 Å, forcing the Ni(II) (ionic radius 0.63 Å) to rest 0.39 Å above the oxygen mean plane. The octahedral ring ions are highly distorted. Long $\text{Ni}^{\text{II}}-\text{N}_{\text{quinHA-pyridyl}}$ and $\text{Ni}^{\text{II}}-\text{O}_{\text{carbonyl}}$ distances are observed (2.160 and 2.175 Å, respectively). Also, the $\text{O}_{\text{carbonyl}}-\text{Ni}^{\text{II}}-\text{N}_{\text{quinHA-pyridyl}}$ angle is 122.19°. For an ideal octahedron, a 90°

Table 2. Structural Parameters for Selected MCs

	Zn ^{II} [12-MC _{Zn^{II},picHA⁻⁴](OTf)_{1.25}(OH)_{0.75}}	Zn ^{II} [12-MC _{Zn^{II},quinHA⁻⁴](BF₄)₂}	Ni ^{II} [12-MC _{Ni^{II},quinHA⁻⁴](NO₃)₂}	Tb ^{III} [12-MC _{Zn^{II},picHA⁻⁴]₂[24-MC_{Zn^{II},picHA⁻⁸](OTf)₃^a}}	Eu ^{II} [15-MC _{Zn^{II},picHA⁻⁵](NO₃)₃}
M _{ring} coord. no.	5	5	6	5	5
av M _{ring} τ	0.21(17)	0.19(13)		0.03(0)	0.30(22)
av M _{ring} -LMP ^b (Å)	0.581(19)	0.534(22)	0.050(15)	0.664(46)	0.510(65)
av M _{ring} -O _{hydroximate} (Å)	2.069(13)	2.068(15)	1.995(12)	2.016(24)	2.053(30)
av M _{ring} -O _{carbonyl} (Å)	2.001(22)	2.006(18)	2.175(20)	2.142(13)	1.998(14)
av M _{ring} -N _{hydroximate} (Å)	2.027(11)	2.021(11)	2.023(13)	2.028(40)	2.014(14)
av M _{ring} -N _{L-py} (Å)	2.152(27) ^c	2.162(31) ^f	2.160(39) ^f	2.170(46) ^c	2.145(28) ^c
av M _{ring} -L _{axial} (Å)	2.044(7)	2.041(3)	2.138(41)	1.981(1)	2.068(18)
av M _{ring} -M _{ring} (Å)	4.813(12)	4.822(2)	4.813(21)	4.870(35)	4.757(67)
av M _{ring} -OMP ^b (Å)	0.707(71)	0.682(161)	0.380(54)	0.564(54)	0.502(326)
central M coord. no.	5	5	5	8	9
av central M-O _{hydroximate} (Å)	2.057(32)	2.041(26)	1.965(9)	2.353(5)	2.422(34)
av central M-OMP _{MC} ^c (Å)	0.325(9)	0.375	0.39	1.075(18)	0.031
central cavity radius ^{d,71} (Å)	0.670(47)	0.646(54)	0.565	0.732(15)	1.099
av M _{ring} -O _{hydroximate} -N _{hydroximate} (deg)	108.89(1.02)	109.70(97)	109.70(0.97)	113.36(54)	107.03(1.00)
av O _{hydroximate} -N _{hydroximate} -C-O _{carbonyl} (deg)	2.71(0.77)	1.09(62)	2.48(1.08)	3.11(43)	0.76(70)
av N _{hydroximate} -C-C-N _{picHA-py} (deg)	7.28(1.83)	9.75(2.67)	5.48(2.77)	3.23(1.57)	5.20(4.57)
av M _{ring} -O _{hydroximate} -N _{hydroximate} -M _{ring} (deg)	163.23(3.24)	162.84(2.82)	162.29(2.01)	173.04(4.12)	166.67(9.35)

^a[12-MC_{Zn^{II},picHA⁻⁴] atoms only. ^bLigand mean plane for five-coordinate ions. ^cOxygen mean plane for the atoms in the central cavity. ^dCavity radius is calculated as the average distance from the oxygen atom to the centroid of the hydroximate oxygen atoms minus the ionic radius of an oxygen atom (1.36 Å). ^eL = picHA. ^fL = quinHA.}

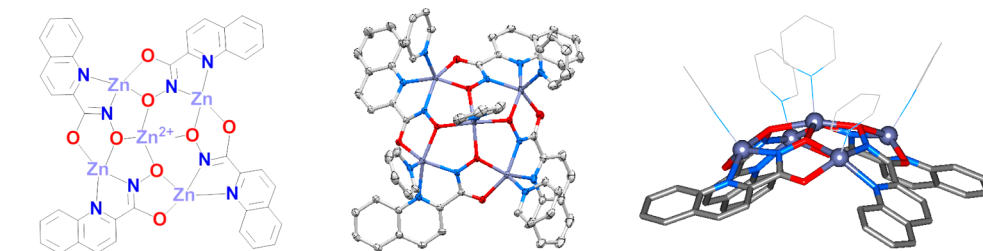


Figure 5. Chemdraw diagram (left) and crystal structure images of the Zn^{II}[12-MC_{Zn^{II},picHA⁻⁴](BF₄)₂ complex viewed down the convex face (thermal ellipsoid plot, center) and from the side (ball and stick diagram, right). Color scheme: gray, carbon; red, oxygen; blue, nitrogen; gray-purple, zinc. Coordinated pyridine ligands are displayed as thin lines in the ball and stick diagram for clarity.}

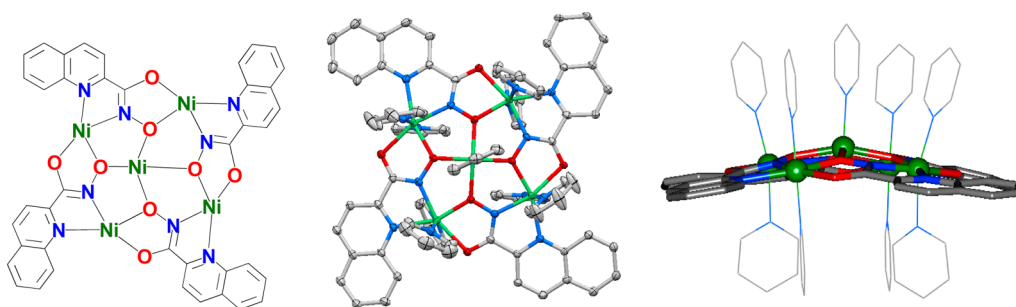


Figure 6. Chemdraw diagram (left) and crystal structure images of the Ni^{II}[12-MC_{Ni^{II},quinHA⁻⁴](NO₃)₂ complex viewed down the convex face (thermal ellipsoid plot, center) and from the side (ball and stick diagram, right). Color scheme: gray, carbon; red, oxygen; blue, nitrogen; green, nickel. Coordinated pyridine ligands are displayed as thin lines in the ball and stick diagram for clarity.}

angle is expected. Other bond distances and angles fall within their expected ranges. ESI-MS supports that Ni^{II}[12-MC_{Ni(II),quinHA⁻⁴](NO₃)₂ is stable in DMSO, acetonitrile, pyridine, methanol, and dimethylformamide. No evidence for structural rearrangements into tetranuclear [6-MC_{Ni^{II},quinHA⁻²] complexes, or any other species, could be found after 24 h at}}

room temperature. Despite significant effort, a crystal structure of the Cu^{II}[12-MC_{Cu^{II},quinHA⁻⁴](NO₃)₂ analogue could not be obtained.}

Solution Stability of the Zn^{II}[12-MC_{Zn^{II},L-4]²⁺ Complexes.} The solution stability of the Zn^{II}[12-MC_{Zn^{II},L-4]²⁺ complexes was examined by ESI-MS and ¹H NMR. Pure}

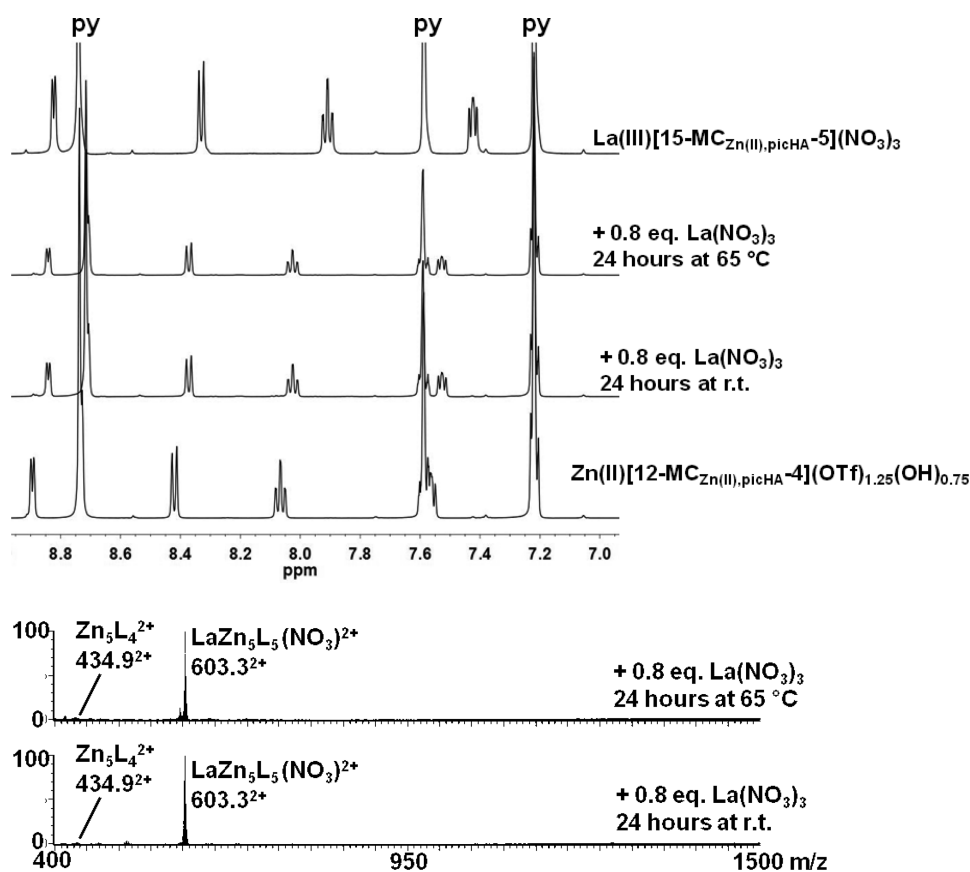


Figure 7. ^1H NMR and ESI-MS spectra of the titration of 0.8 equiv of $\text{La}(\text{NO}_3)_3$ to $\text{Zn}[\text{12-MC}_{\text{Zn}^{\text{II}}}\text{picHA}^{-4}](\text{OTf})_{1.25}(\text{OH})_{0.75}$ in pyridine- d_5 . In the mass spectra, L = picHA.

$\text{Zn}^{\text{II}}[\text{12-MC}_{\text{Zn}^{\text{II}}}\text{picHA}^{-4}](\text{OTf})_{1.25}(\text{OH})_{0.75}$ samples were dissolved in a variety of solvents at room temperature. ESI-MS analysis reveals peaks for $\text{Zn}^{\text{II}}[\text{12-MC}_{\text{Zn}^{\text{II}}}\text{picHA}^{-4}]^{2+}$ are retained in methanol, acetonitrile, and pyridine, and no new high-nuclearity peaks grow in after 24 h. The ^1H NMR spectrum of $\text{Zn}^{\text{II}}[\text{12-MC}_{\text{Zn}^{\text{II}}}\text{picHA}^{-4}](\text{OTf})_{1.25}(\text{OH})_{0.75}$ was collected in pyridine- d_5 (Figure 7). The spectrum contains four resonances in the phenyl region from the MC and three resonances from pyridine. The two doublets and two triplets with 1/1/1/1 integral ratios are consistent with the C_4 -symmetric $\text{Zn}^{\text{II}}[\text{12-MC}_{\text{Zn}^{\text{II}}}\text{picHA}^{-4}]^{2+}$ complex, which has four chemically distinct protons from the picHA ligand. Further evidence for the solution integrity of $\text{Zn}^{\text{II}}[\text{12-MC}_{\text{Zn}^{\text{II}}}\text{picHA}^{-4}]^{2+}$ was obtained from diffusion NMR experiments, which measures the diffusion coefficient of a complex.⁵⁸ The Stokes–Einstein equation (eq 1) relates the diffusion coefficient (D) to the hydrodynamic

$$r_{\text{H}} = \frac{k_{\text{b}}T}{6\pi\eta D} \quad (1)$$

radius of the complex (r_{H}), where k_{b} is the Boltzmann constant (1.3806×10^{-23}), T is the temperature in Kelvin, and η is the viscosity of the solution at that temperature in $\text{kg m}^{-1} \text{s}^{-1}$. The Stokes–Einstein equation calculates the hydrodynamic radius of the complex; therefore, the values are expected to be larger than the molecular radius from the crystal structure. Furthermore, the equation relies on the assumption that the molecule is a perfect sphere, which is a very rough approximation for the $\text{Zn}^{\text{II}}[\text{12-MC}_{\text{Zn}^{\text{II}}}\text{picHA}^{-4}]^{2+}$ complexes with coordinated pyridine ligands. Nevertheless, the hydro-

dynamic radii measured by diffusion NMR are useful data which support the proposition that the complex in the crystal structure is stable in solution.

Diffusion NMR (STE NMR) analysis of $\text{Zn}^{\text{II}}[\text{12-MC}_{\text{Zn}^{\text{II}}}\text{picHA}^{-4}](\text{OTf})_{1.25}(\text{OH})_{0.75}$ gave a diffusion coefficient of $2.8 \pm 0.1 \times 10^{-10} \text{ m}^2 \text{ s}^{-1}$ in methanol- d_4 , corresponding to a hydrodynamic radius of $7.9 \pm 0.3 \text{ \AA}$, consistent with the 8.4 and 7.7 \AA distance from the central $\text{Zn}(\text{II})$ to the furthest hydrogen on the picHA and pyridine ligands, respectively, in the crystal structure. Thus, the STE NMR experiment also supports that the $\text{Zn}^{\text{II}}[\text{12-MC}_{\text{Zn}^{\text{II}}}\text{picHA}^{-4}]^{2+}$ complex is stable in solution. The $\text{Zn}^{\text{II}}[\text{12-MC}_{\text{Zn}^{\text{II}}}\text{quinHA}^{-4}](\text{NO}_3)_2$ complex was also characterized in methanol. ESI-MS showed peaks for $\text{Zn}^{\text{II}}[\text{12-MC}_{\text{Zn}^{\text{II}}}\text{quinHA}^{-4}]^{2+}$ only. ^1H NMR showed six resonances in the phenyl region for the complex, consistent with the C_4 -symmetric complex. The diffusion coefficient of $(4.02 \pm 0.04) \times 10^{-10} \text{ m}^2 \text{ s}^{-1}$ in methanol- d_4 gave a hydrodynamic radius of $10.3 \pm 0.1 \text{ \AA}$, which is consistent with the crystal structure (7.8–10.1 \AA).

Ligand exchange experiments were performed to assess the stability of $\text{Zn}^{\text{II}}[\text{12-MC}_{\text{Zn}^{\text{II}}}\text{L}^{-4}]^{2+}$ further. $\text{Zn}^{\text{II}}[\text{12-MC}_{\text{Zn}^{\text{II}}}\text{picHA}^{-4}](\text{OTf})_{1.25}(\text{OH})_{0.75}$ was mixed with 4 equiv of H_2quinHA in methanol and pyridine, making the picHA/quinHA ratio 1/1. ESI-MS analysis reveals that ligand exchange occurs readily in methanol and pyridine (Figure S3, Supporting Information). A distribution of mixed-ligand $\text{Zn}^{\text{II}}[\text{12-MC}_{\text{Zn}^{\text{II}}}\text{L}^{-4}]^{2+}$ species centered at 3/2 and 2/3 picHA/quinHA ratios were observed after 25 h. As picHA and quinHA are electronically very similar (pK_{a} values of pyridine and quinoline are 5.14 and 4.85, respectively),⁵⁹ this distribution of mixed-ligand $\text{Zn}^{\text{II}}[\text{12-}$

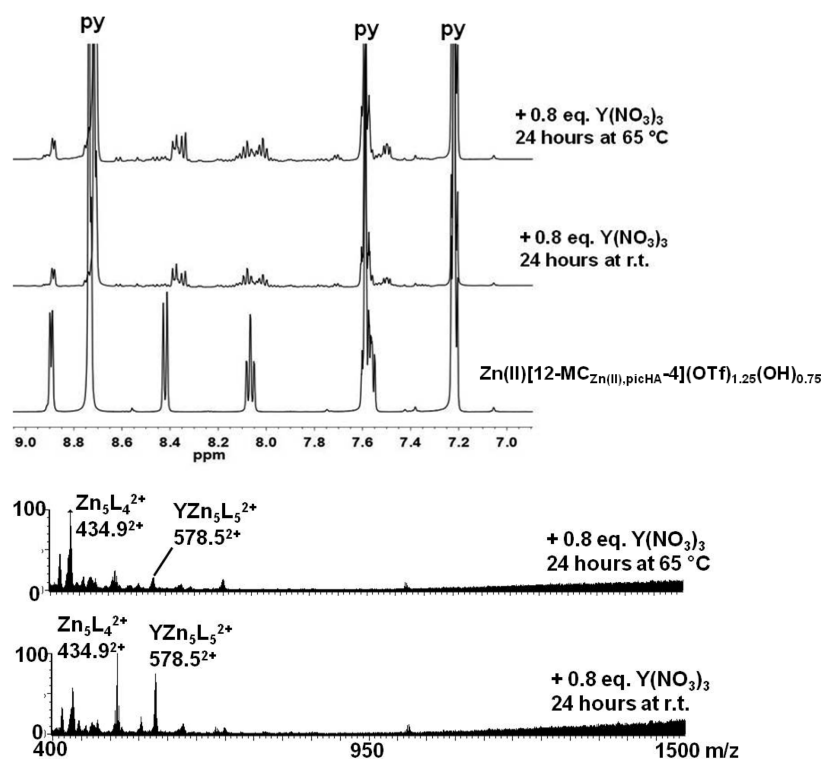


Figure 8. ^1H NMR and ESI-MS spectra of the titration of 0.8 equiv of $\text{Y}(\text{NO}_3)_3$ to $\text{Zn}^{\text{II}}[\text{12-MC}_{\text{Zn}^{\text{II}},\text{picHA}^-4}](\text{OTf})_{1.25}(\text{OH})_{0.75}$ in pyridine- d_5 . In the mass spectra, L = picHA.

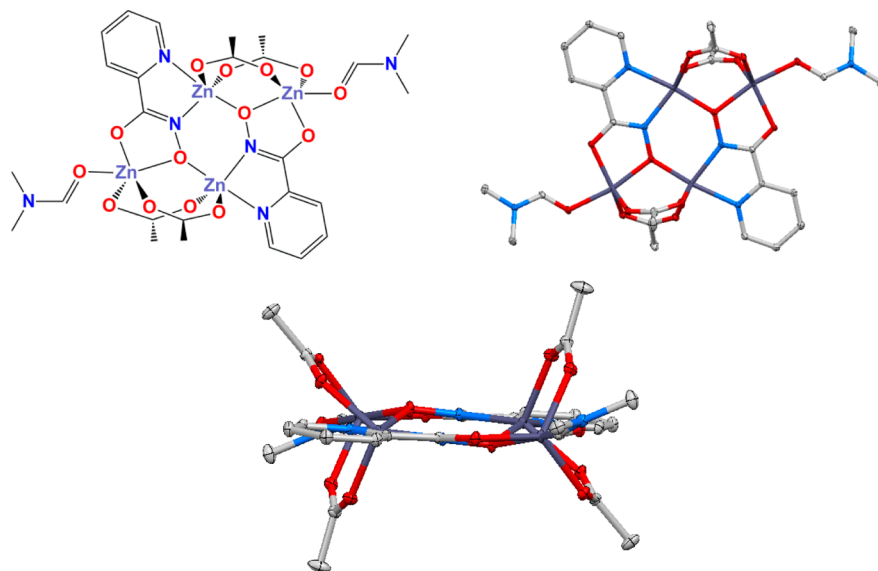


Figure 9. Chemdraw (top left) and thermal ellipsoid plots of the $\text{Zn}_4(\text{picHA})_2(\text{acetate})_4(\text{DMF})_2$ complex viewed perpendicular to the picHA ligand plane and along the plane. Color scheme: gray, carbon; red, oxygen; blue, nitrogen; gray-purple, zinc. Thermal ellipsoids are displayed at the 30% probability level.

$\text{MC}_{\text{Zn}^{\text{II}},\text{L}^-4}^{2+}$ isomers is expected statistically at equilibrium. Thus, complete ligand exchange occurs within 25 h.

Given the extensive carboxylate recognition chemistry of $\text{Ln}^{\text{III}}[\text{15-MC}_{\text{Cu}^{\text{II}},\alpha\text{-aminoHA}^-5}]^{3+}$ complexes, we explored the interaction between $\text{Zn}^{\text{II}}[\text{12-MC}_{\text{Zn}^{\text{II}},\text{picHA}^-4}](\text{OTf})_{1.25}(\text{OH})_{0.75}$, $\text{La}^{\text{III}}[\text{15-MC}_{\text{Zn}^{\text{II}},\text{picHA}^-5}](\text{NO}_3)_3$,²⁹ and $\text{Y}^{\text{III}}[\text{12-MC}_{\text{Zn}^{\text{II}},\text{picHA}^-4}]_2[\text{24-MC}_{\text{Zn}^{\text{II}},\text{picHA}^-8}](\text{OTf})_3$ ¹⁶ with carboxylates. The addition of tetraethylammonium acetate to $\text{Zn}^{\text{II}}[\text{12-MC}_{\text{Zn}^{\text{II}},\text{picHA}^-4}](\text{OTf})_{1.25}(\text{OH})_{0.75}$ reveals changes in the chemical shifts of the $\text{Zn}^{\text{II}}[\text{12-MC}_{\text{Zn}^{\text{II}},\text{picHA}^-4}]^{2+}$ resonances and an increase in the

number of peaks (Figure S4, Supporting Information). The intensity of the $\text{Zn}^{\text{II}}[\text{12-MC}_{\text{Zn}^{\text{II}},\text{picHA}^-4}]^{2+}$ peak in the ESI-MS spectrum with 8 equiv of tetraethylammonium acetate is very low. These NMR and ESI-MS data suggest that acetate can decompose the $\text{Zn}^{\text{II}}[\text{12-MC}_{\text{Zn}^{\text{II}},\text{picHA}^-4}](\text{OTf})_{1.25}(\text{OH})_{0.75}$. The titration of tetraethylammonium acetate to $\text{La}^{\text{III}}[\text{15-MC}_{\text{Zn}^{\text{II}},\text{picHA}^-5}](\text{NO}_3)_3$ in pyridine shows the complete loss of the $\text{La}^{\text{III}}[\text{15-MC}_{\text{Zn}^{\text{II}},\text{picHA}^-5}]^{3+}$ resonances with 5 equiv of acetate (Figure S5, Supporting Information). No peaks for MC ions are observed by ESI-MS, suggesting that this complex is also unstable

respect to carboxylates. No changes to the ^1H NMR or ESI-MS spectrum of the $\text{Y}^{\text{III}}[\text{12-MC}_{\text{Zn}^{\text{II}},\text{picHA-4}}]_2[\text{24-MC}_{\text{Zn}^{\text{II}},\text{picHA-8}}]^{3+}$ are observed with 8 equiv of acetate (Figure S6, Supporting Information); thus, this complex appears to be more stable than $\text{Zn}^{\text{II}}[\text{12-MC}_{\text{Zn}^{\text{II}},\text{picHA-4}}]^{2+}$ and $\text{La}^{\text{III}}[\text{15-MC}_{\text{Zn}^{\text{II}},\text{picHA-5}}]^{3+}$.

Ln(III)-Induced Conversion of $\text{Zn}^{\text{II}}[\text{12-MC}_{\text{Zn}^{\text{II}},\text{picHA-4}}]^{2+}$ to $\text{Ln}^{\text{III}}[\text{15-MC}_{\text{Zn}^{\text{II}},\text{picHA-5}}]^{3+}$. The role of $\text{Zn}^{\text{II}}[\text{12-MC}_{\text{Zn}^{\text{II}},\text{picHA-4}}]^{2+}$ in the assembly of $\text{Ln}^{\text{III}}[\text{15-MC}_{\text{Zn}^{\text{II}},\text{picHA-5}}]^{3+}$ was examined by monitoring the reaction of $\text{Zn}^{\text{II}}[\text{12-MC}_{\text{Zn}^{\text{II}},\text{picHA-4}}](\text{OTf})_{1.25}(\text{OH})_{0.75}$ with a Ln(III) ion. $\text{Zn}^{\text{II}}[\text{12-MC}_{\text{Zn}^{\text{II}},\text{picHA-4}}](\text{OTf})_{1.25}(\text{OH})_{0.75}$ was reacted with 0.8 equiv of either $\text{La}(\text{NO}_3)_3$ or $\text{Y}(\text{NO}_3)_3$, giving a 5/6.25/1 ratio of picHA, Zn(II), and Ln(III). The titration of La(III) to $\text{Zn}^{\text{II}}[\text{12-MC}_{\text{Zn}^{\text{II}},\text{picHA-4}}](\text{OTf})_{1.25}(\text{OH})_{0.75}$ in pyridine at room temperature (Figure 7) shows the $\text{Zn}^{\text{II}}[\text{12-MC}_{\text{Zn}^{\text{II}},\text{picHA-4}}]^{2+}$ resonances are almost completely replaced by four new upfield resonances after 24 h. Heating the solution to 65 °C does not change the spectra, suggesting that equilibrium is reached after 24 h. The spectrum of isolated $\text{La}^{\text{III}}[\text{15-MC}_{\text{Zn}^{\text{II}},\text{picHA-5}}](\text{NO}_3)_3$ in pyridine has the same appearance but slightly different chemical shifts, which is attributed to counterion effects and the excess Zn(II). ESI-MS confirms that $\text{La}^{\text{III}}[\text{15-MC}_{\text{Zn}^{\text{II}},\text{picHA-5}}]^{3+}$ is the product of the reaction. Thus, $\text{Zn}^{\text{II}}[\text{12-MC}_{\text{Zn}^{\text{II}},\text{picHA-4}}]^{2+}$ cleanly converts to $\text{La}^{\text{III}}[\text{15-MC}_{\text{Zn}^{\text{II}},\text{picHA-5}}]^{3+}$ in the presence of $\text{La}(\text{NO}_3)_3$ in pyridine at room temperature. A number of low-intensity peaks appear in the ^1H NMR spectrum upon the addition of $\text{Y}(\text{NO}_3)_3$ to $\text{Zn}^{\text{II}}[\text{12-MC}_{\text{Zn}^{\text{II}},\text{picHA-4}}](\text{OTf})_{1.25}(\text{OH})_{0.75}$ (Figure 8). The $\text{Zn}^{\text{II}}[\text{12-MC}_{\text{Zn}^{\text{II}},\text{picHA-4}}]^{2+}$ resonances are still prominent, and no changes are evident after heating the solution. ESI-MS reveals a variety of species, including $\text{Zn}^{\text{II}}[\text{12-MC}_{\text{Zn}^{\text{II}},\text{picHA-4}}]^{2+}$ and $\text{Y}^{\text{III}}[\text{15-MC}_{\text{Zn}^{\text{II}},\text{picHA-5}}]^{3+}$. Therefore, the conversion of $\text{Zn}^{\text{II}}[\text{12-MC}_{\text{Zn}^{\text{II}},\text{picHA-4}}]^{2+}$ to $\text{Y}^{\text{III}}[\text{15-MC}_{\text{Zn}^{\text{II}},\text{picHA-5}}]^{3+}$ is not as complete or selective as the reaction with La(III), though it still proceeds at room temperature.

Synthesis and Structure of $\text{Zn}_4(\text{picHA})_2(\text{acetate})_4(\text{DMF})_2$. To provide insight into MC decomposition in the presence of acetate, a crystal structure of a $\text{Zn}^{\text{II}}\text{-picHA}$ complex was obtained by the slow evaporation of a methanol/DMF solution. The complex possesses the formula $\text{Zn}_4(\text{picHA})_2(\text{OAc})_4(\text{DMF})_2$ (Figure 9; OAc = acetate, DMF = dimethylformamide) and displays a collapsed MC structure with a $[\text{6-MC}_{\text{Zn}^{\text{II}},\text{picHA-2}}]$ ring. Each Zn(II) ion is five-coordinate, with two monodentate acetate ligands that both bridge an adjacent Zn(II). The acetate-bridged Zn(II) ions are further bridged by an $\text{O}_{\text{hydroximate}}$ atom in the $[\text{6-MC}_{\text{Zn}^{\text{II}},\text{picHA-2}}]$ ring. Two trigonal-bipyramidal Zn(II) ions ($\tau = 0.65$) have bidentate $\text{O},\text{O}'\text{-picHA}$ ligands and a coordinated DMF molecule. The other Zn(II) ions are square pyramidal ($\tau = 0.30$), with a bidentate coordinated $\text{N},\text{N}'\text{-picHA}$ ligand. The $\text{Zn}-\text{N}_{\text{picHA-pyridyl}}$ bond distances are 2.14 Å (Table 3). This complex has also been crystallized with pyridine in place of the DMF molecule.⁶⁰ Synthetically, this complex was frequently obtained during crystallizations containing Ln(III) ions and acetate, demonstrating the need to avoid carboxylates to isolate many $\text{Zn}^{\text{II}}\text{-MCs}$ with picHA ligands. ESI-MS of these reaction mixtures showed peaks for $\text{Ln}^{\text{III}}\text{-MCs}$ and no evidence for $\text{Zn}_4(\text{picHA})_2$. Our attempts to isolate the complex from solutions that did not contain both Ln(III) ions and acetate were unsuccessful. The Ln(III) ion is likely needed to establish the appropriate conditions for crystallizing $\text{Zn}_4(\text{picHA})_2$, though it is highly likely that the complex assembles in solution in the absence of a lanthanide ion.

Table 3. Selected Structural Parameters for $\text{Zn}_4(\text{picHA})_2(\text{OAc})_4(\text{DMF})_2$ and the Previously Reported $\text{Cu}_4(\text{picHA})_4$ ^a

	$\text{Zn}_4(\text{picHA})_2(\text{OAc})_4(\text{DMF})_2$		$\text{Cu}_4(\text{picHA})_2(\text{HpichA})_2(\text{ClO}_4)_2$	
	ring ion 1	ring ion 2	ring ion 1	ring ion 2
ring M coord no.	5	5	4	4
τ	0.649	0.302		
$\text{Zn}_{\text{ring}}\text{-LMP}^b$ (Å)	0.490	0.514	0.26	0.25
$\text{Zn}-\text{O}_{\text{hydroximate}}$ (Å)	2.034	1.988	1.918	1.908, 1.926
$\text{Zn}-\text{O}_{\text{carbonyl}}$ (Å)	2.032		1.914	
$\text{Zn}-\text{N}_{\text{hydroximate}}$ (Å)		2.051	1.960	1.950
$\text{Zn}-\text{N}_{\text{picHA-py}}$ (Å)		2.142	1.893	1.984
$\text{M}-\text{O}_{\text{DMF}}$	2.072			
av $\text{Zn}_{\text{ring}}-\text{O}_{\text{OAc}}$ (Å)	2.005	2.028		
M_1-M_1 (Å)		3.289		3.333
M_2-M_2 (Å)		4.012		3.908
M_1-M_2 (Å)		7.303		7.141
$\text{M}-\text{O}-\text{N}$ angle (deg)	112.08	128.96	110.25	128.22
$\text{M}_1-\text{O}-\text{M}_2$ angle (deg)		109.71		120.20
$\text{M}_2-\text{O}-\text{N}-\text{M}_2$ torsion angle (deg)		25.61		9.58
picHA $\text{O}-\text{C}-\text{C}-\text{O}$ torsion angle	3.33		1.59	7.19
picHA $\text{N}-\text{C}-\text{C}-\text{N}$ torsion angle		7.86	0.21	1.66

^aFor both complexes, ring ion #1 is located towards the periphery of the molecule, while ring ion #2 is located in the 6-MC-2 ring. ^bLMP = ligand mean plane.

ESI-MS of the $\text{Zn}_4(\text{picHA})_2(\text{acetate})_4(\text{DMF})_2$ species dissolved in methanol, pyridine, DMF, or DMSO after 24 h do not contain peaks from a $\text{Zn}_4(\text{picHA})_2(\text{OAc})_4$ species. Peaks for $\text{Zn}^{\text{II}}[\text{12-MC}_{\text{Zn}^{\text{II}},\text{picHA-4}}]^{2+}$ are observed, suggesting that this complex undergoes a structural rearrangement to some extent at room temperature. It should be noted that $\text{Zn}_4(\text{picHA})_2(\text{OAc})_4$ is a neutral complex and might not ionize effectively; therefore, the lack of any signal in the ESI mass spectrum should not be taken as proof that the complex does not persist in solution. The ^1H NMR spectrum in pyridine-*d*₅ (Figure 10) contains three prominent resonances for a species

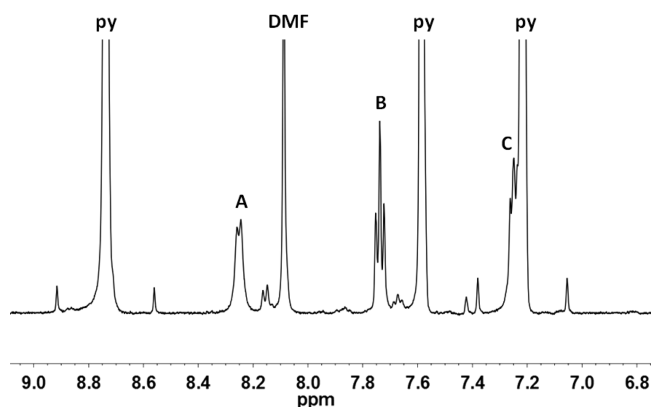


Figure 10. ^1H NMR spectrum of the $\text{Zn}_4(\text{picHA})_2(\text{OAc})_4(\text{DMF})_2$ complex dissolved in pyridine-*d*₅ after 24 h. Peaks A–C correspond to picHA resonances arising from a molecule with a hydrodynamic radius that is much larger than that of the free ligand on the basis of STE NMR (A and B resonances gave $r_{\text{H}} = 6.6 \pm 0.3$ Å).

with picHA at 8.26, 7.74, and 7.22 ppm, the last overlapping with the pyridine resonance (peaks A–C in Figure 10, respectively). The integral ratios of the DMF and acetate resonances to picHA are slightly greater than expected for the intact $\text{Zn}_4(\text{picHA})_2(\text{acetate})_4(\text{DMF})_2$, suggesting that other minor picHA species exist. Low-intensity peaks are also seen for different species in the phenyl region, supporting the partial $\text{Zn}_4(\text{picHA})_2(\text{OAc})_4(\text{DMF})_2$ rearrangement seen by ESI-MS. The diffusion coefficient for peaks A and B measured by STE NMR was measured as $(3.3 \pm 0.1) \times 10^{-10} \text{ m}^2 \text{ s}^{-1}$ in pyridine- d_5 at 20 °C, corresponding to a hydrodynamic radius of $6.6 \pm 0.3 \text{ \AA}$. The radii from the crystal structure are 6.0 and 7.1 Å, respectively. Since $\text{Zn}_4(\text{picHA})_2(\text{OAc})_4$ is planar and the Stokes–Einstein equation makes the assumption of a spherical particle, the $6.6 \pm 0.3 \text{ \AA}$ value seems reasonable for the $\text{Zn}_4(\text{picHA})_2(\text{OAc})_4$ complex. The acetate resonance gave a hydrodynamic radius of 4.5 Å. If the acetate were fully complexed with the $\text{Zn}_4(\text{picHA})_2$ complex, the hydrodynamic radius from the acetate resonance would be the same as the picHA resonances. It is likely that the acetate resonance contains an overlapping signal from uncoordinated acetate, acetate coordinated to free Zn(II), and acetate in the $\text{Zn}_4(\text{picHA})_2$ complex. The diffusion coefficient and hydrodynamic radii from the DMF resonances were consistent with an uncoordinated DMF ligand. As a whole, the NMR data support the model that $\text{Zn}_4(\text{picHA})_2(\text{OAc})_4$ persists in solution to some extent, while rearrangement to other species also occurs.

DISCUSSION

Our aim with this work is to develop new information on the assembly of lanthanide metallocrowns, and multicomponent assemblies in general, by studying the coordination chemistry of M(II)-hydroximate intermediates. On the basis of the $[\text{12-MC}_{\text{Zn}^{\text{II}},\text{picHA}-4}]$ motif in $\text{Ln}^{\text{III}}[\text{12-MC}_{\text{Zn}^{\text{II}},\text{picHA}-4}]_2[\text{24-MC}_{\text{Zn}^{\text{II}},\text{picHA}-8}](\text{OTf})_3$ complexes,¹⁶ we suspected that the elusive $\text{M}^{\text{II}}[\text{12-MC}_{\text{M}^{\text{II}},\text{picHA}-4}]^{2+}$ could be isolated with Zn(II) ring ions. Our hypothesis was upheld in this work. $\text{Zn}^{\text{II}}[\text{12-MC}_{\text{Zn}^{\text{II}},\text{picHA}-4}]^{2+}$ assembles readily in pyridine, and its crystal structure was obtained with both picHA and quinHA ligands. Initial crystals of $\text{Zn}^{\text{II}}[\text{12-MC}_{\text{Zn}^{\text{II}},\text{picHA}-4}](\text{OTf})_{1.25}(\text{OH})_{0.75}$ contained up to 10% triethylammonium impurities on the basis of ¹H NMR. The $\text{Zn}^{\text{II}}[\text{12-MC}_{\text{Zn}^{\text{II}},\text{picHA}-4}](\text{OTf})_{1.25}(\text{OH})_{0.75}$ sample contained less than 1% triethylammonium after recrystallization, albeit with a roughly 20% decrease in the overall yield. Isolation of the $\text{Zn}^{\text{II}}[\text{12-MC}_{\text{Zn}^{\text{II}},\text{quinHA}-4}]^{2+}$ complexes was more straightforward. The complex crystallized readily with NO_3^- and BF_4^- counterions in reasonable yields. A crystal structure with Ni(II) was also obtained. $\text{Ni}^{\text{II}}[\text{12-MC}_{\text{Ni}^{\text{II}},\text{quinHA}-4}](\text{NO}_3)_2$ was most effectively isolated as an amorphous powder from hot pyridine solutions.

The crystal structures of the $\text{M}^{\text{II}}[\text{12-MC}_{\text{M}^{\text{II}},\text{L}-4}]^{2+}$ complexes with Zn(II) and Ni(II) provide the first direct experimental evidence for the bowl-shaped topology predicted by Tegoni et al.⁴⁵ The $\text{M}^{\text{II}}[\text{12-MC}_{\text{M}^{\text{II}},\text{L}-4}]^{2+}$ forms because its central cavity is complementary with the size of the divalent transition metal. The $\sim 1.05 \text{ \AA}$ central cavity of $[\text{15-MC}_{\text{M}^{\text{II}},\text{L}-5}]$ is too large for a divalent transition metal. The bowl shape arises in $\text{M}^{\text{II}}[\text{12-MC}_{\text{M}^{\text{II}},\text{L}-4}]^{2+}$ because the 4-fold symmetric assembly must inherently orient the metal ions at 90° angles relative to each other. Ligand field effects in the d^8 Ni(II) ions force $\text{Ni}^{\text{II}}[\text{12-MC}_{\text{Ni}^{\text{II}},\text{quinHA}-4}](\text{NO}_3)_2$ to be more planar than the Zn(II) analogue (cavity depths 1.3 and 4.8 Å, respectively). The

relative planarity of the Ni(II) complex is most evident in the structural overlay of the $\text{M}^{\text{II}}[\text{12-MC}_{\text{M}^{\text{II}},\text{quinHA}-4}]^{2+}$ complexes (Figure 11). $\text{Eu}^{\text{III}}[\text{15-MC}_{\text{M}^{\text{III}},\text{picHA}-5}](\text{NO}_3)_3$ complexes are

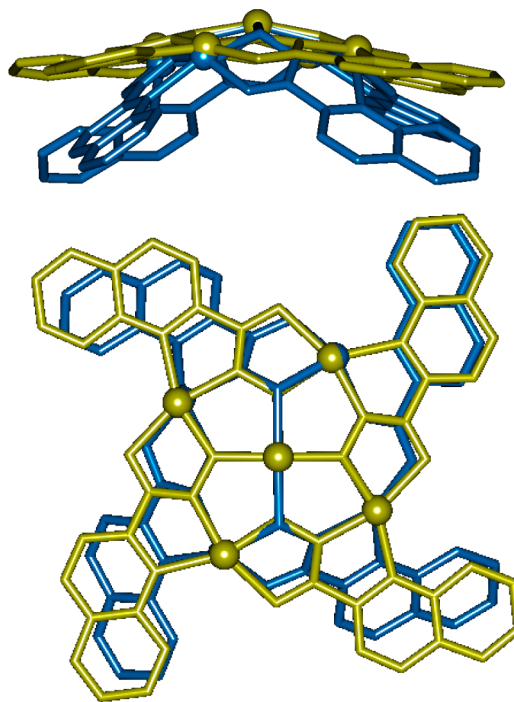


Figure 11. Structural overlay of $\text{Zn}^{\text{II}}[\text{12-MC}_{\text{Zn}^{\text{II}},\text{quinHA}-4}](\text{BF}_4)_2$ (turquoise) and $\text{Ni}^{\text{II}}[\text{12-MC}_{\text{Ni}^{\text{II}},\text{quinHA}-4}](\text{NO}_3)_2$ (yellow). The structures are tethered at the four hydroximate oxygen atoms.

progressively more planar from Zn(II) to Cu(II) to Ni(II).²⁹ On the basis of this trend, our hypothesis is that the $\text{Cu}^{\text{II}}[\text{12-MC}_{\text{Cu}^{\text{II}},\text{L}-4}]^{2+}$ has planarity intermediate between those of the Ni(II) and Zn(II) analogues. Supporting this point, an overlay of Tegoni's calculated $\text{Cu}^{\text{II}}[\text{12-MC}_{\text{Cu}^{\text{II}},\text{valHA}-4}]^{2+}$ structure with the $\text{M}^{\text{II}}[\text{12-MC}_{\text{Cu}^{\text{II}},\text{quinHA}-4}]^{2+}$ complexes with Ni(II) shows that the Cu(II) complex has intermediate planarity.

As the ideal angles in the picHA and quinHA chelate rings orient the metal ions at 108°, the chelate rings in the square $\text{M}^{\text{II}}[\text{12-MC}_{\text{M}^{\text{II}},\text{L}-4}]^{2+}$ undergo structural perturbations at each ring metal to accommodate this 18° difference. Analysis of the $\text{Zn}^{\text{II}}[\text{12-MC}_{\text{Zn}^{\text{II}},\text{L}-4}]^{2+}$ crystal structures reveal a number of prominent structural distortions (Table 2). The average angle between the centroid of the O,O' -picHA chelate, Zn(II), and the axial pyridyl nitrogen in $\text{Zn}^{\text{II}}[\text{12-MC}_{\text{Zn}^{\text{II}},\text{quinHA}-4}](\text{BF}_4)_2$ is 111.1°, while the ideal planar complex would have a 90° angle. The $\text{Zn}-\text{O}_{\text{hydroximate}}-\text{N}_{\text{hydroximate}}-\text{Zn}$ torsion angle is 162.9° in $\text{Zn}^{\text{II}}[\text{12-MC}_{\text{Zn}^{\text{II}},\text{quinHA}-4}](\text{BF}_4)_2$, in comparison to 180° in the ideal planar molecule. Also, there is an increase in the $\text{Zn}^{\text{II}}-\text{N}_{\text{picHA-pyridyl}}$ bond distance to over 2.15 Å. These parameters reveal that the square-shaped macrocycle is generated through bending at the ring ions, twisting of the picHA face, and an elongation in the $\text{Zn}^{\text{II}}-\text{N}_{\text{picHA-pyridyl}}$ bond distance. In effect, the concavity of the $\text{Zn}^{\text{II}}[\text{12-MC}_{\text{Zn}^{\text{II}},\text{L}-4}]^{2+}$ motif eliminates the influence of the picHA chelate ring geometry. A similar effect was observed in $[\text{9-MC}-3]$ complexes with salicylhydroxamic acid (shi^{3-}), which are also bowl-shaped.^{10,61,62} The chelate rings of this ligand are arranged at a 90° internal angle; therefore, shi^{3-} frequently generates $\text{M}^{\text{N}}[\text{12-MC}_{\text{M}^{\text{N}},\text{shi}^{3-}-4}]$ complexes.^{11,63} The $\text{Ni}^{\text{II}}[\text{12-MC}_{\text{Ni}^{\text{II}},\text{quinHA}-4}](\text{NO}_3)_2$ is more

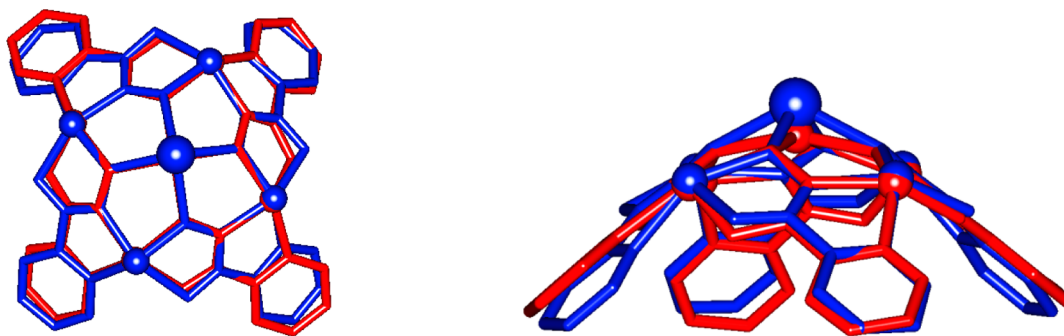


Figure 12. Structural overlay of the $\text{Zn}^{\text{II}}[12\text{-MC}_{\text{Zn}^{\text{II}},\text{picHA-4}}](\text{OTf})_{1.25}(\text{OH})_{0.75}$ (red) and $[12\text{-MC}_{\text{Zn}^{\text{II}},\text{picHA-4}}]$ frameworks of the previously reported $\text{Tb}^{\text{III}}[12\text{-MC}_{\text{Zn}^{\text{II}},\text{picHA-4}}]_2[24\text{-MC}_{\text{Zn}^{\text{II}},\text{picHA-8}}](\text{OTf})_3$ (blue). The structures are tethered at the four hydroxamate oxygen atoms.

planar through compression in the center and elongation at the periphery. Such structural perturbations are evident in the small central cavity radius and long $\text{Ni}^{\text{II}}\text{-O}_{\text{carbonyl}}$ distances and $\text{O}_{\text{carbonyl}}\text{-Ni}^{\text{II}}\text{-N}_{\text{quinHA-pyridyl}}$ angles.

Comparison of the $\text{Zn}^{\text{II}}[12\text{-MC}_{\text{Zn}^{\text{II}},\text{picHA-4}}](\text{OTf})_{1.25}(\text{OH})_{0.75}$ structure with that of $\text{Tb}^{\text{III}}[12\text{-MC}_{\text{Zn}^{\text{II}},\text{picHA-4}}]_2[24\text{-MC}_{\text{Zn}^{\text{II}},\text{picHA-8}}](\text{OTf})_3$ ¹⁶ addresses how the topology of the metallamacrocycle is perturbed by the size of the central ion. The ionic radii of the five-coordinate $\text{Zn}(\text{II})$ and eight-coordinate $\text{Tb}(\text{III})$ are 0.68 and 1.040 Å, respectively. An overlay of the two structures (Figure 12) and analysis of their bond distances and angles (Table 2) reveals more similarities than differences. The most distinct difference is that the $\text{Tb}(\text{III})$ central ion resides 0.75 Å further above the hydroxamate oxygen mean plane than the central $\text{Zn}(\text{II})$. This difference arises because the small $[12\text{-MC}_{\text{Zn}^{\text{II}},\text{picHA-4}}]$ central cavity better accommodates $\text{Zn}(\text{II})$ (ionic radius 0.68 Å⁶⁴). The bond distances, bond angles, and pitch of the ligands on $\text{Zn}^{\text{II}}[12\text{-MC}_{\text{Zn}^{\text{II}},\text{picHA-4}}](\text{OTf})_{1.25}(\text{OH})_{0.75}$ and $\text{Tb}^{\text{III}}[12\text{-MC}_{\text{Zn}^{\text{II}},\text{picHA-4}}]_2[24\text{-MC}_{\text{Zn}^{\text{II}},\text{picHA-8}}](\text{OTf})_3$ are quite similar. Due to the differences in the axial ligands on the ring metals in the two structures, we cannot ascertain how the steepness of the concave face is influenced by the central ion from these structures. The similarity speaks to the robustness of the concave $\text{M}^{\text{N}}[12\text{-MC}_{\text{Zn}^{\text{II}},\text{L-4}}]$ motif, as it can accommodate small divalent and large trivalent cations with minimal perturbations to its structure. This observation is in marked contrast to $[12\text{-MC}_{\text{Cu}^{\text{II}},\text{L-4}}]$, which is extremely difficult to isolate and has not been observed with trivalent cations.

The concavity of $\text{Zn}^{\text{II}}[12\text{-MC}_{\text{Zn}^{\text{II}},\text{L-4}}]^{2+}$ could lead to different functionality than the planar $\text{M}^{\text{N}}[12\text{-MC}_{\text{M}^{\text{N}},\text{L-4}}]$ complexes with shi^{3-} and other ligands.^{11,63,65} First, only one face of the concave $\text{Zn}^{\text{II}}[12\text{-MC}_{\text{Zn}^{\text{II}},\text{picHA-4}}](\text{OTf})_{1.25}(\text{OH})_{0.75}$ has open coordination sites. This is important when considering assemblies or networks of these MCs. For planar $\text{M}^{\text{N}}[12\text{-MC}_{\text{M}^{\text{N}},\text{L-4}}]$ complexes, bridging guests coordinate to both faces of the complex, leading to the formation of infinite chains or networks.^{22,66} Similarly, the $\text{Ln}^{\text{III}}[15\text{-MC}_{\text{Cu}^{\text{II}},\alpha\text{-aminoHA-5}}]^{3+}$ complexes bind anionic guests to both the hydrophobic and hydrophilic faces.^{34,35} The concave $\text{Zn}^{\text{II}}[12\text{-MC}_{\text{Zn}^{\text{II}},\text{L-4}}]^{2+}$ complexes can only coordinate Lewis bases to one face, which favors the formation of *discrete* assemblies. It should be noted that the more planar $\text{Ni}^{\text{II}}[12\text{-MC}_{\text{Ni}^{\text{II}},\text{quinHA-4}}](\text{NO}_3)_2$ binds pyridyl ligands on both faces of the MC. Thus, this face selectivity in $\text{M}^{\text{II}}[12\text{-MC}_{\text{M}^{\text{II}},\text{L-4}}]^{2+}$ complexes will vary with the coordination preferences of the metal ions. Nearly all face recognition should be lost with the $\text{Cu}(\text{II})$ complex.

The concave $\text{Zn}^{\text{II}}[12\text{-MC}_{\text{Zn}^{\text{II}},\text{L-4}}]^{2+}$ will also have cation recognition behavior different from that of planar $\text{M}^{\text{N}}[12\text{-MC}_{\text{M}^{\text{N}},\text{L-4}}]$ complexes. A number of planar $\text{M}^{\text{N}}[12\text{-MC}_{\text{M}^{\text{N}},\text{L-4}}]$ complexes bind cations on both faces of the MC, such as the $\text{Na}(\text{I})_3[12\text{-MC}_{\text{Ga}(\text{III}),\text{shi-4}}]_2$ metallacryptate¹² and monomeric $\text{M}^{\text{I}}_2[12\text{-MC}_{\text{Mn}^{\text{III}},\text{shi-4}}]^+$ complexes.⁶⁷ On the basis of a simple Lewis model, the oxygen lone pairs in a planar MC are oriented above and below the MC plane, leading to cation binding on *both* faces. In contrast, the lone pairs on the bowl-shaped $\text{Zn}^{\text{II}}[12\text{-MC}_{\text{Zn}^{\text{II}},\text{L-4}}]^{2+}$ are oriented to the *same* face of the MC. One lone pair should be pointed toward the center of the MC on the convex face, while the other is oriented above the convex face and toward the periphery of the MC. Thus, the bowl-shaped $\text{Zn}^{\text{II}}[12\text{-MC}_{\text{Zn}^{\text{II}},\text{L-4}}]^{2+}$ should be *incapable* of binding cations on the concave face and only one central cation is possible.

The molecular recognition capabilities of the concave face of the $\text{Zn}^{\text{II}}[12\text{-MC}_{\text{Zn}^{\text{II}},\text{L-4}}]^{2+}$ complexes are also promising. The concave face has a cavitand topology, similar to that of a calixarene or resorcinarene.⁶⁸ It is likely that the concave MC will exhibit similar molecular recognition chemistry for noncoordinating organic guests as these benchmark supramolecular hosts. The crystal structure of $\text{Zn}^{\text{II}}[12\text{-MC}_{\text{Zn}^{\text{II}},\text{picHA-4}}]^{2+}$ shows a methanol molecule held at van der Waals distances in the center of the concave cavity (Figure S1, Supporting Information). $\text{Zn}^{\text{II}}[12\text{-MC}_{\text{Zn}^{\text{II}},\text{quinHA-4}}]^{2+}$ contains two pyridine molecules (Figure S2, Supporting Information). The molecular recognition chemistry of the $\text{Ni}(\text{II})$ analogue is likely limited due to the planarity of the complex. The recognition of noncoordinating organic guests would be a new area for MC host–guest chemistry, which has focused primarily on Lewis acids and bases.

Stability and Reactivity of $\text{Zn}^{\text{II}}[12\text{-MC}_{\text{Zn}^{\text{II}},\text{L-4}}]^{2+}$. The solution stability of $\text{M}^{\text{II}}[12\text{-MC}_{\text{M}^{\text{II}},\text{L-4}}]^{2+}$ complexes ($\text{M} = \text{Cu}(\text{II}), \text{Ni}(\text{II})$) and their reactivity to form $\text{Ln}^{\text{III}}[15\text{-MC}_{\text{M}^{\text{II}},\text{L-5}}]^{3+}$ complexes is well established.^{38,40,42,69} Therefore, the solution behavior of $\text{Ni}^{\text{II}}[12\text{-MC}_{\text{Ni}^{\text{II}},\text{quinHA-4}}](\text{NO}_3)_2$ was not investigated in depth, though it does appear to be reasonably stable in solution. $\text{Zn}^{\text{II}}[12\text{-MC}_{\text{Zn}^{\text{II}},\text{L-4}}]^{2+}$ is stable in the surveyed organic solvents at room temperature on the basis of ESI-MS and ¹H NMR (Figures 3 and 7), with no new peaks appearing over 24 h. This stability suggests promise for utilizing $\text{Zn}^{\text{II}}[12\text{-MC}_{\text{Zn}^{\text{II}},\text{L-4}}]^{2+}$ in molecular recognition applications. Unfortunately, $\text{Zn}^{\text{II}}[12\text{-MC}_{\text{Zn}^{\text{II}},\text{L-4}}]^{2+}$ decomposes in the presence of acetate on the basis of ESI-MS and ¹H NMR (Figure S4, Supporting Information). Such decomposition is presumably due to the formation of stable acetate-bridged polynuclear

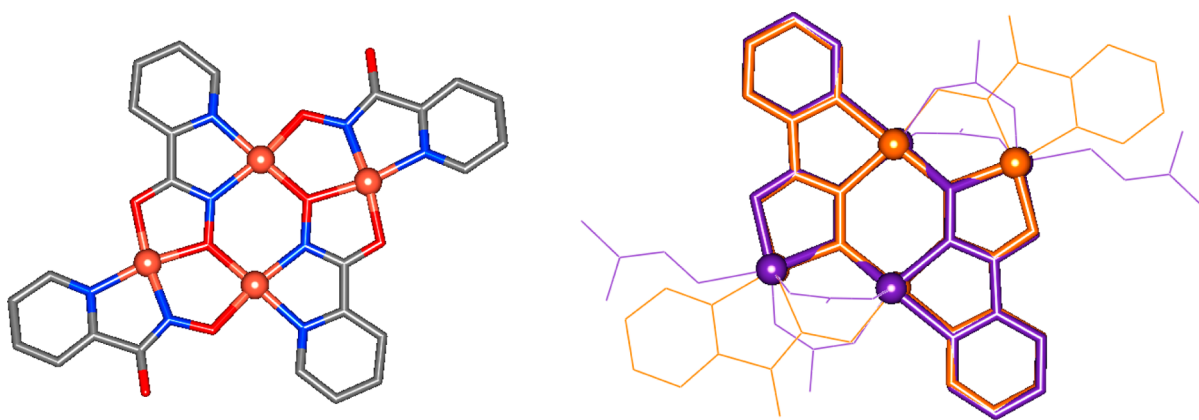


Figure 13. Image of the $\text{Cu}_4(\text{picHA})_2(\text{HpicHA})_2(\text{ClO}_4)_2$ structure reported by Fritsky et al. (right) and structural overlays of $\text{Cu}_4(\text{picHA})_2(\text{HpicHA})_2(\text{ClO}_4)_2$ (orange) and $\text{Zn}_4(\text{picHA})_2(\text{OAc})_4(\text{DMF})_2$ (purple) that highlight the similar picHA coordination and central $[\text{6-MC}_{\text{M}^{\text{II}},\text{picHA}-2}]$ motif. The structures in the overlay image are tethered at the hydroximate carbons and the phenyl carbons *para* to the hydroximate. Color scheme: gray, carbon; red, oxygen; blue, nitrogen; orange, copper.

Zn(II) complexes, such as the tetranuclear $\text{Zn}_4(\text{picHA})_2(\text{OAc})_4$ complex (Figure 9).

To gain further insight into the kinetic and thermodynamic stability of $\text{Zn}^{\text{II}}[\text{12-MC}_{\text{Zn}^{\text{II}},\text{L}-4}]^{2+}$ as well as its role as an intermediate in the assembly of $\text{Ln}^{\text{III}}[\text{15-MC}_{\text{Zn}^{\text{II}},\text{L}-5}]^{3+}$, the complex was reacted with $\text{La}(\text{NO}_3)_3$ and $\text{Y}(\text{NO}_3)_3$. ^1H NMR and ESI-MS suggest that $\text{Zn}^{\text{II}}[\text{12-MC}_{\text{Zn}^{\text{II}},\text{picHA}-4}](\text{OTf})_{1.25}(\text{OH})_{0.75}$ converts readily to $\text{La}^{\text{III}}[\text{15-MC}_{\text{Zn}^{\text{II}},\text{L}-5}]^{3+}$ at room temperature. No other peaks are observed that indicate side products or intermediates (Figure 7). Conversion to $\text{Y}^{\text{III}}[\text{15-MC}_{\text{Zn}^{\text{II}},\text{L}-5}]^{3+}$ also proceeds readily at room temperature, though it does not proceed to completion (Figure 8). Unfortunately, these data do not clarify whether $\text{Zn}^{\text{II}}[\text{12-MC}_{\text{Zn}^{\text{II}},\text{picHA}-4}]^{2+}$ is the specific intermediate that reacts with the Ln(III) ion to form $\text{Ln}^{\text{III}}[\text{15-MC}_{\text{Zn}^{\text{II}},\text{picHA}-5}]^{3+}$. The rearrangement of $\text{Zn}^{\text{II}}[\text{12-MC}_{\text{Zn}^{\text{II}},\text{L}-4}]^{2+}$ to $\text{Ln}^{\text{III}}[\text{15-MC}_{\text{Zn}^{\text{II}},\text{picHA}-5}]^{3+}$ requires disruption of at least two five-membered chelate rings to split open $\text{Zn}^{\text{II}}[\text{12-MC}_{\text{Zn}^{\text{II}},\text{L}-4}]^{2+}$. A pathway where $\text{Zn}^{\text{II}}[\text{12-MC}_{\text{Zn}^{\text{II}},\text{L}-4}]^{2+}$ is a precursor for the species that reacts with the Ln(III) ion requires the disruption of at least three five-membered chelate rings. On the basis of this qualitative picture, the pathway where $\text{Zn}^{\text{II}}[\text{12-MC}_{\text{Zn}^{\text{II}},\text{L}-4}]^{2+}$ is the intermediate seems more likely, given that its activation barrier should be lower. Notably, the instability of $\text{Zn}^{\text{II}}[\text{12-MC}_{\text{Zn}^{\text{II}},\text{picHA}-4}]^{2+}$ to carboxylates and the observation of rapid ligand exchange suggest that a reaction pathway involving disruption of the $\text{Zn}^{\text{II}}[\text{12-MC}_{\text{Zn}^{\text{II}},\text{L}-4}]^{2+}$ ring is energetically feasible.

The titrations of $\text{Ln}(\text{NO}_3)_3$ to $\text{Zn}^{\text{II}}[\text{12-MC}_{\text{Zn}^{\text{II}},\text{picHA}-4}]^{2+}$ also show that $\text{Zn}^{\text{II}}[\text{12-MC}_{\text{Zn}^{\text{II}},\text{picHA}-4}]^{2+}$ has a thermodynamic stability similar to that of $\text{Ln}^{\text{III}}[\text{15-MC}_{\text{Zn}^{\text{II}},\text{picHA}-5}]^{3+}$. The conversion to $\text{La}^{\text{III}}[\text{15-MC}_{\text{Zn}^{\text{II}},\text{picHA}-5}]^{3+}$ is nearly complete in pyridine, though faint peaks for $\text{Zn}^{\text{II}}[\text{12-MC}_{\text{Zn}^{\text{II}},\text{picHA}-4}]^{2+}$ remain with 1 equiv of $\text{La}(\text{NO}_3)_3$. The conversion is much more limited with Y(III), revealing a greater thermodynamic stability for $\text{Ln}^{\text{III}}[\text{15-MC}_{\text{Zn}^{\text{II}},\text{picHA}-5}]^{3+}$ with larger lanthanides. This trend is also present in $\text{Ln}^{\text{III}}[\text{15-MC}_{\text{Cu}^{\text{II}},\text{pheHA}-5}]$ complexes in aqueous conditions.⁷⁰ The similar trend in $\text{Ln}^{\text{III}}[\text{15-MC}_{\text{M}^{\text{II}},\text{L}-5}]$ stability seen in macrocycles with Zn(II) and Cu(II) ring ions is unsurprising from a structural standpoint. $\text{Ln}^{\text{III}}[\text{15-MC}_{\text{M}^{\text{II}},\text{picHA}-5}]$ complexes with different ring ions provide very similar ligand environments for the central Ln(III) ion.²⁹

The observation of residual $\text{Zn}^{\text{II}}[\text{12-MC}_{\text{Zn}^{\text{II}},\text{picHA}-4}]^{2+}$ in the Ln(III) ion titrations suggests that $\text{Zn}^{\text{II}}[\text{12-MC}_{\text{Zn}^{\text{II}},\text{picHA}-4}]^{2+}$ and $\text{Ln}^{\text{III}}[\text{15-MC}_{\text{Zn}^{\text{II}},\text{picHA}-5}]^{3+}$ have comparable thermodynamic stabilities, which is in contrast with the trend for Cu(II) and Ni(II) ring metals. Thermodynamic investigations of these systems with α -aminoHA ligands under aqueous conditions have shown that $\text{Cu}^{\text{II}}[\text{12-MC}_{\text{Cu}^{\text{II}},\alpha\text{-aminoHA}-4}]^{2+}$ and $\text{Ni}^{\text{II}}[\text{12-MC}_{\text{Ni}^{\text{II}},\alpha\text{-aminoHA}-4}]^{2+}$ possess modest thermodynamic stability, persisting at equilibrium with a variety of mononuclear species from pH 4 to 6.^{40,45} The NMR and ESI-MS spectra of $\text{Zn}^{\text{II}}[\text{12-MC}_{\text{Zn}^{\text{II}},\text{L}-4}]^{2+}$ suggest that the MC is the only species in pyridine at room temperature. Thus, $\text{M}^{\text{II}}[\text{12-MC}_{\text{M}^{\text{II}},\text{L}-4}]^{2+}$ seems to be most stable with Zn(II). This can be rationalized on the basis of the preferred geometries of the ions. As $\text{Zn}^{\text{II}}[\text{12-MC}_{\text{Zn}^{\text{II}},\text{L}-4}]^{2+}$ is a concave structure, it requires metal ions with distorted-square-pyramidal geometries. As ligand field effects promote square-planar and octahedral geometries in Cu(II) and Ni(II), $\text{M}^{\text{II}}[\text{12-MC}_{\text{M}^{\text{II}},\text{L}-4}]^{2+}$ should be less stable thermodynamically with these metal ions. Notably, $\text{Cu}^{\text{II}}[\text{12-MC}_{\text{Cu}^{\text{II}},\text{pheHA}-4}]^{2+}$ is much less stable than the corresponding $\text{La}^{\text{III}}[\text{15-MC}_{\text{Cu}^{\text{II}},\text{pheHA}-5}]^{3+}$. Effectively no $\text{Cu}^{\text{II}}[\text{12-MC}_{\text{Cu}^{\text{II}},\text{pheHA}-4}]^{2+}$ is present at equilibrium upon dissolution of $\text{La}^{\text{III}}[\text{15-MC}_{\text{Cu}^{\text{II}},\text{pheHA}-5}]^{3+}$. In contrast, the La(III) ion titrations suggest that $\text{Zn}^{\text{II}}[\text{12-MC}_{\text{Zn}^{\text{II}},\text{picHA}-4}]^{2+}$ persists at equilibrium with the $\text{La}^{\text{III}}[\text{15-MC}_{\text{Zn}^{\text{II}},\text{picHA}-5}]^{3+}$. Therefore, the difference in the relative stabilities of the MCs is greater with Cu(II) than with Zn(II). This could be due to both the greater stability of $\text{Zn}^{\text{II}}[\text{12-MC}_{\text{Zn}^{\text{II}},\text{L}-4}]^{2+}$ relative to $\text{Cu}^{\text{II}}[\text{12-MC}_{\text{Cu}^{\text{II}},\text{L}-4}]^{2+}$ and the lower stability of $\text{Ln}^{\text{III}}[\text{15-MC}_{\text{Zn}^{\text{II}},\text{L}-5}]^{3+}$ relative to $\text{Ln}^{\text{III}}[\text{15-MC}_{\text{Cu}^{\text{II}},\text{L}-5}]^{3+}$.

Comparison of Tetranuclear $[\text{6-MC}_{\text{M}^{\text{II}},\text{picHA}-2}]$ Complexes with Cu(II) and Zn(II). The central $[\text{6-MC}_{\text{Zn}^{\text{II}},\text{picHA}-2}]$ topology of the tetranuclear cluster resembles the structural motifs found in a number of hydroximate complexes of Cu(II) and Mn(III),^{47,48} particularly a $\text{Cu}_4(\text{picHA})_2(\text{HpicHA})_2(\text{ClO}_4)_2$ complex reported by Fritsky et al.⁴⁶ The Cu(II) ions in this complex possess square-planar geometry, and the complex as a whole is quite planar. The overlay of $\text{Cu}_4(\text{picHA})_2(\text{HpicHA})_2^{2+}$ and $\text{Zn}_4(\text{picHA})_2(\text{OAc})_4(\text{DMF})_2$ displayed in Figure 13 demonstrates the similarity of the tetranuclear cores. The metal–metal distances are remarkably similar (Table 3), as are the $\text{M}^{\text{II}}\text{–N–O}$ angles. Differences between the $[\text{6-MC}_{\text{M}^{\text{II}},\text{picHA}-2}]$ cores of the two structures arise

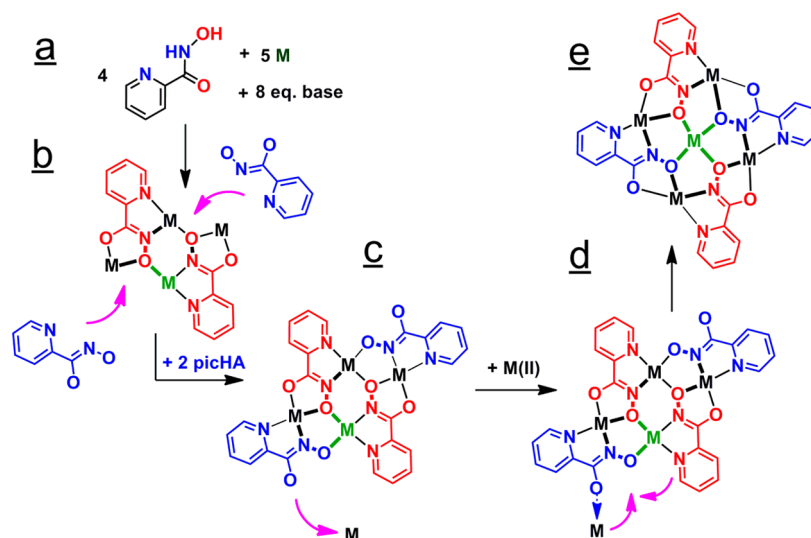


Figure 14. Scheme of a possible assembly pathway for four picHA ligands and five ring metals to form $M^{II}[12-MC_{M^{II},picHA-4}]^{2+}$ that invokes the structurally characterized tetranuclear $[6-MC_{M^{II},picHA-2}]$ complexes. Bonds in the core $M^{II}-N-O$ repeating unit of the final $M^{II}[12-MC_{M^{II},L-4}]^{2+}$ macrocycle are displayed with a bold line, while those to the central ion are displayed in green. The central $M(II)$ ion is displayed in green, the core M_4L_2 ligands are displayed in red, and the exogenous ligands in the M_4L_4 are displayed in blue.

from different coordination numbers of the metal ions. The five-coordinate Zn(II) ions have longer bond distances than the four-coordinate Cu(II). Unlike the Cu(II) ions, the Zn(II) ions reside above the ligand mean plane, leading the complex as a whole to be nonplanar (Figure 13).

Other obvious differences between $Cu_4(picHA)_2(HpicHA)_2^{2+}$ and $Zn_4(picHA)_2(OAc)_4(DMF)_2$ are the peripheral ligands. The μ_2 -acetate and DMF ligands on $Zn_4(picHA)_2(OAc)_4(DMF)_2$ are needed to satisfy the preference of Zn(II) ions for five-coordinate geometries with picHA. The μ_2 -acetate forms a three-atom bridge between adjacent Zn(II) ions. In contrast, $Cu_4(picHA)_2(HpicHA)_2^{2+}$ has a two-atom hydroximate bridge between the adjacent Cu(II) ions. The different coordination geometries of the Zn(II) and Cu(II) ions might also explain the different bridging ligands. Presumably, picHA would be capable of bridging those peripheral Zn(II) ions to form a $Zn_4(picHA)_4$ species. However, such a complex was not observed by crystallography or by ESI-MS. It is likely that $M^{II}[12-MC_{M^{II},L-4}]^{2+}$ is particularly stable with Zn(II) due to its preferred distorted-square-pyramidal geometry. Thus, $Zn^{II}[12-MC_{Zn^{II},L-4}]^{2+}$ does not readily rearrange to a tetranuclear $[6-MC_{Zn^{II},L-2}]$ complex unless an excess of acetate ligands is present. In contrast, the planar $[6-MC_{M^{II},L-2}]$ is more readily generated with Cu(II) because its preferred coordination geometries align picHA ligands in an equatorial plane.

Currently little is known about the assembly mechanism for $M^{II}[12-MC_{M^{II},L-4}]^{2+}$ complexes, and many chemically reasonable pathways can be envisioned. The prevailing mechanism invokes the central metal ion as a core template that is then wrapped with M^{II} -hydroximate units to generate the macrocycle. It has also been proposed that a vacant $[12-MC_{M^{II},L-4}]^{2+}$ could assemble and encapsulate the central metal ion. While electronic repulsion between the $O_{hydroximate}$ lone pairs in the central cavity might inhibit the formation of such an intermediate, experimental evidence of a vacant $[15-MC_{Ni^{II},alaHA-5}]$ from Tegoni et al. loosely supports this possibility.⁴⁰

The structural characterization of $Zn_4(picHA)_2(OAc)_4(DMF)_2$ and $Cu_4(picHA)_4$ ⁴⁶ has led us to propose an alternative mechanism for $M^{II}[12-MC_{M^{II},L-4}]^{2+}$ assembly (Figure 14). This proposed mechanism is meant to complement the other possible pathways. The current experimental data on $M^{II}[12-MC_{M^{II},L-4}]^{2+}$ assembly cannot definitively affirm or refute any of the mechanisms. Moreover, the assembly could reasonably proceed through multiple pathways, given the complexity of the M^{II} -hydroximate equilibria and the low activation energy for making and breaking dative bonds with Ni(II), Cu(II), and Zn(II). This mechanism identifies $M^{II}[12-MC_{M^{II},L-4}]^{2+}$ as the thermodynamically favored product. This assumption is supported by extensive potentiometry investigations under aqueous conditions.^{40–42,44,45} Moreover, $M^{II}[12-MC_{M^{II},L-4}]^{2+}$ contains a macrocyclic motif and more five-membered chelate rings than the tetranuclear $[6-MC_{M^{II},L-2}]$ species, which should make it the more stable species.

We feel that the peculiar methods required to isolate $Zn_4(picHA)_2$ and $Cu_4(picHA)_4$ should not discredit the role of the $[6-MC_{M^{II},L-2}]$ complexes as intermediates in $M^{II}[12-MC_{M^{II},L-4}]^{2+}$ assembly. Previously, $Cu_4(picHA)_4$ species were isolated by dissolving crystalline $Cu^{II}[12-MC_{Cu^{II},picHA-4}](ClO_4)_2$ in organic solvents.⁴⁶ While $Cu^{II}[12-MC_{Cu^{II},picHA-4}]^{2+}$ should be the most stable species, $Cu_4(picHA)_4$ could form under these conditions on the basis of it persisting as minor species at equilibrium and/or the kinetically driven disassembly of the $Cu^{II}[12-MC_{Cu^{II},picHA-4}](ClO_4)_2$ complex. It seems reasonable that $M(II)[12-MC_{M^{II},picHA-4}]^{2+}$ assembly is kinetically reversible at room temperature because Ni(II), Cu(II), and Zn(II) are labile ions and the Zn(II) analogue undergoes rapid ligand exchange. Isolation of $Cu_4(picHA)_4$ after $Cu_5(picHA)_4$ dissolution would therefore be a result of reaching the appropriate crystallization conditions and not a chemical reaction where $Cu_4(picHA)_4$ is the thermodynamically favored product. Also of note, though the $Zn_4(picHA)_2$ was only isolated in the presence of a Ln(III) ion, invoking the complex as an intermediate in the mechanism is reasonable, since the complex should be expected to assemble in solution in the

absence of a Ln(III) ion. Difficulty observing the $[6\text{-MC}_{M^u,L-2}]$ species by ESI-MS can be attributed to poor ionization of the neutral complexes and the fact that they might persist at low concentrations.

PicHA or α -aminoHA ligands and divalent transition metals (Figure 14a) are known to form a variety of mononuclear species.³⁸ The first high-nuclearity species proposed to assemble is the tetranuclear $[6\text{-MC}_{M^u,L-2}]$ depicted in Figure 14b, which resembles $\text{Zn}_4(\text{picHA})_2(\text{OAc})_4(\text{DMF})_2$ (Figure 9). In this intermediate, one $M^u\text{-N-O}$ linkage in the $[6\text{-MC}_{M^u,L-2}]$ ring will be present in the final $M^u[12\text{-MC}_{M^u,L-4}]^{2+}$. Also, the resulting central metal is present, though only one dative bond with the $\text{O}_{\text{hydroximate}}$ in the final structure has been formed. From this intermediate, two exogenous ligands coordinate to form the tetranuclear $[6\text{-MC}_{M^u,L-2}]$ depicted in Figure 14c, which possesses the $\text{Cu}_4(\text{picHA})_4$ structure (Figure 13).⁴⁶ Next, an exogenous metal ion can coordinate to the open carbonyl ligand, forming the species in Figure 14d with M_3L_4 stoichiometry. A close contact between the hydrogen atom ortho to the pyridyl nitrogen forces exo coordination to the $\text{O}_{\text{carbonyl}}$ in a planar complex, which is expected for M_4L_4 . This monodentate coordination mode likely has very modest stability, and this complex would be in rapid equilibrium with M_4L_4 . Finally, an ML_2 unit shifts within the M_3L_4 to form $M^u[12\text{-MC}_{M^u,L-4}]^{2+}$, depicted in Figure 14e. During this step, the monodentate exocoordinated metal ion on $\text{O}_{\text{carbonyl}}$ is proposed to shift to a bidentate endo coordination. This can be facilitated by the complex adopting a nonplanar morphology, which would allow interaction with the open $\text{O}_{\text{hydroximate}}$ site without forming a close contact with the picHA hydrogen atom. This transition from intermediate d to intermediate e would likely have the highest activation energy, as it involves the disruption of four dative bonds.

CONCLUSIONS

The first crystallographically characterized $M^u[12\text{-MC}_{M^u,L-4}]^{2+}$ complexes with a ligand from the picHA/ α -aminoHA family were obtained with Zn(II) and Ni(II) metal ions. $\text{Zn}^u[12\text{-MC}_{\text{Zn}^u,\text{picHA}-4}]^{2+}$ appears to have stability comparable to that of $\text{Ln}^{\text{III}}[15\text{-MC}_{\text{Ln}^{\text{III}},\text{picHA}-5}]^{3+}$, which is due in part to the square-pyramidal Zn(II) ions favoring the concave $\text{Zn}^u[12\text{-MC}_{\text{Zn}^u,\text{picHA}-4}]^{2+}$ topology. The Cu(II) analogues have different stability because ligand field effects disfavor the formation of a concave $\text{Cu}^u[12\text{-MC}_{\text{Cu}^u,\text{picHA}-4}]^{2+}$. Conventional design strategies for preparing stable lanthanide MCs have focused on positive design approaches, such as the use of symmetry-compatible ligands and metal ions to promote the formation of one complex. These results suggest that negative design approaches for destabilizing intermediates in the assembly should be considered to ensure that only the lanthanide MC persists at equilibrium.

$\text{Zn}_4(\text{picHA})_2(\text{OAc})_4(\text{DMF})_2$ joins $\text{Cu}_4(\text{picHA})_4$ and $\text{Cu}_{28}(\text{norvalHA})_{20}$ as complexes with tetranuclear $[6\text{-MC}_{M^u,L-2}]$ motifs obtained in organic solvents from ligands in the picHA/ α -aminoHA family. This work further alludes to the importance of these motifs in metallacrown assembly equilibria. Previous thermodynamic studies on solutions of α -amino hydroxamic acids and divalent transition metals were performed in aqueous solutions, not in organic solutions where the tetranuclear $[6\text{-MC}_{M^u,L-2}]$ complexes have been obtained. It is likely that the tetranuclear $[6\text{-MC}_{M^u,L-2}]$ complexes are not thermodynamically or kinetically stable under aqueous conditions, though they are stable in organic solvents.

Furthermore, ESI-MS could be ineffective at detecting the presence of tetranuclear $[6\text{-MC}_{M^u,L-2}]$ complexes because they might not ionize effectively, even though they persist in solution. We propose that these tetranuclear $[6\text{-MC}_{M^u,L-2}]$ complexes are intermediates in the assembly of $M^u[12\text{-MC}_{M^u,L-4}]^{2+}$ complexes.

The $M^u[12\text{-MC}_{M^u,L-4}]^{2+}$ and tetranuclear $[6\text{-MC}_{M^u,L-2}]$ complexes are perhaps most interesting from the viewpoint of their role as intermediates in the assembly of lanthanide MCs. These assembly results with $\text{Zn}^u[12\text{-MC}_{\text{Zn}^u,\text{picHA}-4}]^{2+}$ and previous results with Cu(II) and Ni(II) do not prove conclusively that $M^u[12\text{-MC}_{M^u,L-4}]$ reacts with a Ln(III) ion directly to form the resulting $\text{Ln}^{\text{III}}[15\text{-MC}_{M^u,L-5}]$. It is possible that only low-nuclearity M(II) complexes react with the lanthanide ion, and $M^u[12\text{-MC}_{M^u,L-4}]$ is a mistake in the assembly process. Further experiments would be needed to clarify the role of $M^u[12\text{-MC}_{M^u,L-4}]$ and tetranuclear $[6\text{-MC}_{M^u,L-2}]$ species in lanthanide MC formation.

Lanthanide MCs, such as the $\text{Ln}^{\text{III}}[15\text{-MC}_{M^u,L-5}]^{3+}$ complexes, are unique supramolecular hosts because, unlike crown ethers, the lanthanide guest is typically necessary to template the macrocycle. It is reasonable to consider that a variety of host-guest complexes with different structural motifs could be generated on the basis of which intermediate binds the lanthanide guest. Control over the reactivity of transition-metal-ligand intermediates could allow for the synthesis of different lanthanide MCs with enhanced magnetic, luminescent, and molecular recognition properties. Presumably, factors such as the solvent, pH, and anions could influence the stability of the various intermediates, such as the $M^u[12\text{-MC}_{M^u,L-4}]^{2+}$ and tetranuclear $[6\text{-MC}_{M^u,L-2}]$, and control the assembly of a specific lanthanide metallacrown. Further information on the speciation and stability of complexes from transition-metal ions and MC forming ligands would aid these endeavors.

ASSOCIATED CONTENT

Supporting Information

Figures giving additional structural and characterization data and CIF files giving crystallographic data. This material is available free of charge via the Internet at <http://pubs.acs.org>.

AUTHOR INFORMATION

Corresponding Author

*V.L.P.: e-mail, vlpec@umich.edu; tel, (734) 763-1519.

Notes

The authors declare no competing financial interest.

ACKNOWLEDGMENTS

We thank the National Science Foundation for funding of MC research (CHE-1057331) and X-ray diffraction instrumentation (CHE-0840456). Dr. Matteo Tegoni is acknowledged for helpful discussions.

REFERENCES

- (1) Chakrabarty, R.; Mukherjee, P. S.; Stang, P. J. *Chem. Rev.* **2011**, *111*, 6810–918.
- (2) Yoshizawa, M.; Klosterman, J. K.; Fujita, M. *Angew. Chem., Int. Ed.* **2009**, *48*, 3418–38.
- (3) Cangelosi, V. M.; Carter, T. G.; Zakharov, L. N.; Johnson, D. W. *Chem. Commun.* **2009**, 5606–8.
- (4) Safont-Sempere, M. M.; Fernandez, G.; Wurthner, F. *Chem. Rev.* **2011**, *111*, 5784–814.

- (5) Mezei, G.; Zaleski, C. M.; Pecoraro, V. L. *Chem. Rev.* **2007**, *107*, 4933–5003.
- (6) Pecoraro, V. L.; Stemmler, A. J.; Gibney, B. R.; Bodwin, J. J.; Wang, H.; Kampf, J. W.; Barwinski, A. In *Progress in Inorganic Chemistry*; Karlin, K. D., Ed.; Wiley: New York, 1997; Vol. 45.
- (7) Lah, M. S.; Pecoraro, V. L. *Inorg. Chem.* **1991**, *30*, 878–880.
- (8) Gibney, B. R.; Wang, H.; Kampf, J. W.; Pecoraro, V. L. *Inorg. Chem.* **1996**, *35*, 6184–3193.
- (9) Beckett, R.; Hoskins, B. F. *J. Chem. Soc., Dalton Trans.* **1972**, 291–295.
- (10) Pecoraro, V. L. *Inorg. Chim. Acta* **1989**, *155*, 171–173.
- (11) Lah, M. S.; Pecoraro, V. L. *J. Am. Chem. Soc.* **1989**, *111*, 7258–7259.
- (12) Lah, M. S.; Gibney, B. R.; Tierney, D. L.; Penner-Hahn, J. E.; Pecoraro, V. L. *J. Am. Chem. Soc.* **1993**, *115*, 5857–5858.
- (13) Zaleski, C. M.; Depperman, E. C.; Kampf, J. W.; Kirk, M. L.; Pecoraro, V. L. *Angew. Chem., Int. Ed.* **2004**, *43*, 3912–4.
- (14) Zaleski, C. M.; Kampf, J. W.; Mallah, T.; Kirk, M. L.; Pecoraro, V. L. *Inorg. Chem.* **2007**, *46*, 1954–1956.
- (15) Zaleski, C. M.; Depperman, E. C.; Dendrinou-Samara, C.; Alexiou, M.; Kampf, J. W.; Kessissoglou, D. P.; Kirk, M. L.; Pecoraro, V. L. *J. Am. Chem. Soc.* **2005**, *127*, 12862–12872.
- (16) Jankolovits, J.; Andolina, C. M.; Kampf, J. W.; Raymond, K. N.; Pecoraro, V. L. *Angew. Chem., Int. Ed.* **2011**, *50*, 9660–4.
- (17) Severin, K. *Coord. Chem. Rev.* **2003**, *245*, 3–10.
- (18) Jones, L. F.; Kilner, C. A.; Halcrow, M. A. *Chem. Eur. J.* **2009**, *15*, 4667–75.
- (19) Pavlishchuk, A. V.; Kolotilov, S. V.; Zeller, M.; Thompson, L. K.; Fritsky, I. O.; Addison, A. W.; Hunter, A. D. *Eur. J. Inorg. Chem.* **2010**, *2010*, 4851–4858.
- (20) Moon, M.; Kim, I.; Lah, M. S. *Inorg. Chem.* **2000**, *39*, 2710–2711.
- (21) Pecoraro, V. L.; Bodwin, J. J.; Cutland, A. D. *J. Solid State Chem.* **2000**, *152*, 68–77.
- (22) Pavlishchuk, A. V.; Kolotilov, S. V.; Zeller, M.; Shvets, O. V.; Fritsky, I. O.; Lofland, S. E.; Addison, A. W.; Hunter, A. D. *Eur. J. Inorg. Chem.* **2011**, *2011*, 4826–4836.
- (23) MC nomenclature in this work follows the format $M^N[\text{ring size-}MC_{M',L}^N]$ of ring oxygen atoms], where M is the central ion with N oxidation state, M' is the central ion with N' oxidation state, and L is the ligand. The counterion or the overall charge of the MC is given after the brackets when referring to a specific complex.
- (24) Stemmler, A. J.; Kampf, J. W.; Pecoraro, V. L. *Angew. Chem., Int. Ed. Engl.* **1996**, *35*, 2841–2843.
- (25) Stemmler, A. J.; Barwinski, A.; Baldwin, M. J.; Young, V.; Pecoraro, V. L. *J. Am. Chem. Soc.* **1996**, *118*, 11962–11963.
- (26) Stemmler, A. J.; Kampf, J. W.; Kirk, M. L.; Atasi, B. H.; Pecoraro, V. L. *Inorg. Chem.* **1999**, *38*, 2807–2817.
- (27) Seda, S. H.; Janczak, J.; Lisowski, J. *Inorg. Chem. Commun.* **2006**, *9*, 792–796.
- (28) Seda, S. H.; Janczak, J.; Lisowski, J. *Eur. J. Inorg. Chem.* **2007**, *2007*, 3015–3022.
- (29) Jankolovits, J.; Kampf, J. W.; Pecoraro, V. L. *Polyhedron* **2013**, *52*, 491–499.
- (30) Zaleski, C. M.; Depperman, E. C.; Kampf, J. W.; Kirk, M. L.; Pecoraro, V. L. *Inorg. Chem.* **2006**, *45*, 10022–10024.
- (31) Lim, C.-S.; Jankolovits, J.; Zhao, P.; Kampf, J. W.; Pecoraro, V. L. *Inorg. Chem.* **2011**, *50*, 4832–4841.
- (32) Grant, J. T.; Jankolovits, J.; Pecoraro, V. L. *Inorg. Chem.* **2012**, *51*, 8034–8041.
- (33) Tegoni, M.; Tropiano, M.; Marchio, L. *Dalton Trans.* **2009**, 6705–6708.
- (34) Cutland, A. D.; Halfen, J. A.; Kampf, J. W.; Pecoraro, V. L. *J. Am. Chem. Soc.* **2001**, *123*, 6211–6212.
- (35) Jankolovits, J.; Lim, C.-S.; Mezei, G.; Kampf, J. W.; Pecoraro, V. L. *Inorg. Chem.* **2012**, *51*, 4527–4538.
- (36) Mezei, G.; Kampf, J. W.; Pan, S.; Poepelmeier, K. R.; Watkins, B.; Pecoraro, V. L. *Chem. Commun.* **2007**, 1148–50.
- (37) Lim, C. S.; Jankolovits, J.; Kampf, J. W.; Pecoraro, V. L. *Chem. Asian J.* **2010**, *5*, 46–49.
- (38) Tegoni, M.; Remelli, M. *Coord. Chem. Rev.* **2012**, *256*, 289–315.
- (39) Gokel, G. W.; Echegoyen, L.; Kim, M. S.; Eyring, E. M.; Petrucci, S. *Biophys. Chem.* **1987**, *26*, 225–233.
- (40) Bacco, D.; Bertolasi, V.; Dallavalle, F.; Galliera, L.; Marchetti, N.; Marchio, L.; Remelli, M.; Tegoni, M. *Dalton Trans.* **2011**, *40*, 2491–2501.
- (41) Dallavalle, F.; Tegoni, M. *Polyhedron* **2001**, *20*, 2697–2704.
- (42) Careri, M.; Dallavalle, F.; Tegoni, M.; Zagnoni, I. *J. Inorg. Biochem.* **2003**, *93*, 174–180.
- (43) Seda, S. H.; Janczak, J.; Lisowski, J. *Inorg. Chim. Acta* **2006**, *359*, 1055–1063.
- (44) Dallavalle, F.; Remelli, M.; Sansone, F.; Bacco, D.; Tegoni, M. *Inorg. Chem.* **2010**, *49*, 1761–72.
- (45) Tegoni, M.; Remelli, M.; Bacco, D.; Marchio, L.; Dallavalle, F. *Dalton Trans.* **2008**, 2693–2701.
- (46) Golenya, I. A.; Gumienna-Kontacka, E.; Boyko, A. N.; Haukka, M.; Fritsky, I. O. *Inorg. Chem.* **2012**, *51*, 6221–6227.
- (47) Johnson, J. A.; Kampf, J. W.; Pecoraro, V. L. *Angew. Chem., Int. Ed.* **2003**, *42*, 546–549.
- (48) Saarinen, H.; Orama, M.; Korvenranta, J. *Acta Chem. Scand.* **1989**, *43*, 834.
- (49) Psomas, G.; Stemmler, A. J.; Dendrinou-Samara, C.; Bodwin, J. J.; Schneider, M.; Alexiou, M.; Kampf, J. W.; Kessissoglou, D. P.; Pecoraro, V. L. *Inorg. Chem.* **2001**, *40*, 1562–1570.
- (50) CrystalClear 2.0; Rigaku Corp., Tokyo, Japan.
- (51) Sheldrick, G. M. *Acta Crystallogr.* **2008**, *A64*, 112–122.
- (52) SAINT; Bruker Analytical X-ray, Madison, WI, 2009.
- (53) Sheldrick, G. M. *SADABS: Program for Empirical Absorption Correction of Area Detector Data*, University of Göttingen, Göttingen, Germany, 2008.
- (54) Sheldrick, G. M. *Acta Crystallogr.* **2008**, *A64*, 112–122.
- (55) Addison, A. W.; Rao, T. N.; Reedijk, J.; van Rijn, J.; Verschoor, G. C. *J. Chem. Soc., Dalton Trans.* **1984**, 1349.
- (56) Kersting, B.; Lehmann, U. *Adv. Inorg. Chem.* **2009**, *61*, 407–470.
- (57) Frischmann, P. D.; Maclachlan, M. J. *Chem. Soc. Rev.* **2012**, *42*, 871–890.
- (58) Cohen, Y.; Avram, L.; Frish, L. *Angew. Chem., Int. Ed.* **2005**, *44*, 520–54.
- (59) Braud, E. A.; Nachod, F. C. *Determination of Organic Structures by Physical Methods*; Academic Press: New York, 1955.
- (60) Unit cell parameters: 8.495 × 10.285 × 10.537 Å, 89.40 × 85.06 × 70.09°, volume 862.22 Å³.
- (61) Lah, M. S.; Kirk, M. L.; Hatfield, W.; Pecoraro, V. L. *J. Chem. Soc., Chem. Commun.* **1989**, 1606–1608.
- (62) Gibney, B. R.; Stemmler, A. J.; Pilotek, S.; Kampf, J. W.; Pecoraro, V. L. *Inorg. Chem.* **1993**, *32*, 6008–6015.
- (63) Gibney, B. R.; Kessissoglou, D. P.; Kampf, J. W.; Pecoraro, V. L. *Inorg. Chem.* **1994**, *33*, 4840–4849.
- (64) Shannon, R. D. *Acta Crystallogr.* **1976**, *A32*, 751–767.
- (65) Tegoni, M.; Ferretti, L.; Sansone, F.; Remelli, M.; Bertolasi, V.; Dallavalle, F. *Chem. Eur. J.* **2007**, *13*, 1300–8.
- (66) Bodwin, J. J.; Pecoraro, V. L. *Inorg. Chem.* **2000**, *39*, 3434–3435.
- (67) Kessissoglou, D. P.; Bodwin, J. J.; Kampf, J.; Dendrinou-Samara, C.; Pecoraro, V. L. *Inorg. Chim. Acta* **2002**, *331*, 73–80.
- (68) Cram, D. J.; Cram, J. M. In *Container Molecules and Their Guests*; Stoddart, J. F., Ed.; Royal Society of Chemistry: London, 1994.
- (69) Pacco, A.; Parac-Vogt, T. N.; Besien, E. v.; Pierloot, K.; Gorler-Walrand, C.; Binnemans, K. *Eur. J. Inorg. Chem.* **2005**, 3305–3310.
- (70) Tegoni, M.; Furlotti, M.; Tropiano, M.; Lim, C.-S.; Pecoraro, V. L. *Inorg. Chem.* **2010**, *49*, 5190–5201.
- (71) Zaleski, C. M.; Lim, C.-S.; Cutland-Van Noord, A. D.; Kampf, J. W.; Pecoraro, V. L. *Inorg. Chem.* **2011**, *50*, 7707–17.